Journal of Catalysis 368 (2018) 411–426

Contents lists available at ScienceDirect

Journal of Catalysis

journal homepage: www.elsevier.com/locate/jcat

Mechanism and site requirements for thiophene hydrodesulfurization on supported Re domains in metal or sulfide form

Edwin Yik, Enrique Iglesia *

Department of Chemical and Biomolecular Engineering, University of California, Berkeley, CA 94720, USA
Chemical Sciences Division, E.O. Lawrence Berkeley National Laboratory, Berkeley, CA 94720, USA

ARTICLE INFO

Article history:
Received 19 October 2017
Revised 15 March 2018
Accepted 28 March 2018
Available online 21 June 2018

Keywords:
Re
ReS_x
ReS_2
Thiophene hydrodesulfurization
C—S bond activation
C—S bond scission

ABSTRACT

The elementary steps and active structures involved in thiophene hydrodesulfurization (HDS) are examined here through structural and functional assessments of Re and ReS_x catalysts prepared from ReO_x precursors by treatment in H_2 or H_2S. These samples retain their respective bulk phases at sulfur chemical potentials prevalent during HDS, because nucleation barriers inhibit the interconversion of isotropic Re metal and lamellar ReS_x layers. HDS turnover rates were much higher on ReS_x than Re, but both phases showed similar kinetic effects of thiophene, H_2, and H_2S and binding constants for adsorbed thiophene and S-atoms, consistent with a common mechanism involving active sites that differ in number but not in binding properties. In such elementary steps, the surface consists of a template of refractory S-atoms that are bound irreversibly, known to form even at H_2S/H_2 ratios much lower than in HDS practice. Interstices within such templates can reversibly bind reactive intermediates, thus allowing catalytic turnovers, and act as HDS active sites. The number of such interstices depends on M—S bond strength, which is lower for particles with ReS_x than with Re bulk phases; their binding properties, however, are not dictated by the bulk phase, because they consist of those surface spaces that become capable of binding S-species weakly enough to allow their formation and removal as part of each catalytic turnover. On both Re and ReS_x, thiophene conversion rates are limited by the addition of one H-atom to bound thiophene to form intermediate species that give tetrahydrothiophene (THT) and C_4 hydrocarbons at a kinetic branch after this kinetically-relevant step. Thiophene pressures and H_2S/H_2 ratios do not influence THT/C_4 product ratios, which decrease as residence time increases because of secondary C—S cleavage in THT to form C_4 products. Both products form in a single surface sojourn at similar site coverages by intermediates, as is also the case for secondary THT reactions. The effects of H_2 on these primary and secondary events indicate that the kinetic branching occurs at a bound intermediate with the H-content of dihydrothiophene, from which the C—S bond cleavage transition state is also formed. As in C—C and C—O cleavage, C—S bond scission requires H-removal from saturated reactants (THT) by (i) increasing the bond order of its surface attachment; (ii) weakening the C—X bond being cleaved (X = C, O, S); and (iii) evolving H_2 to minimize entropy losses upon formation of the transition state.

1. Introduction

Catalytic hydrodesulfurization (HDS) is the reaction by which sulfur atoms are removed from organosulfur compounds through the cleavage of carbon-sulfur bonds. Such reactions have been extensively studied on transition metal sulfides [1–3]. The structure and reactivity of Co-Mo and Ni-W sulfides [3–10] have attracted particular attention because of their broad deployment in heteroatom removal from refinery streams in processes required to produce fuels that meet stringent specifications for heteroatom content [11,12]. HDS rates on such catalyst systems [1,13–23] are seldom reported as turnover rates, a measure of intrinsic reactivity that requires reliable counts of active sites. O_2 uptakes after a specific reductive treatment [24–26] are often used for such purposes, but oxygen atoms merely titrate S-vacancies formed by such reductive treatments, thus reflecting the lability of S-atoms in metal sulfides instead of a rigorous count of exposed active sites. The occasional claims of reactivity correlations with O_2 uptakes reflect the expected effects of M—S bond energies on redox cycles that are limited by the availability of S-vacancies on stoichiometric sulfides, but such O_2 uptakes cannot be used to compare intrinsic reactivity among diverse catalyst compositions or to determine whether rate improvements reflect changes in the number or the

---

* Corresponding author.
E-mail address: iglesia@berkeley.edu (E. Iglesia).

https://doi.org/10.1016/j.jcat.2018.03.031
0021-9517/

reactivity of active sites. The structural and compositional complexity of layered sulfides has precluded accurate assessments of turnover rates, while their non-uniform and anisotropic nature has often led to contradictory claims about reaction mechanisms, about how reactivity and selectivity depend on composition and structural properties, and about the nature and number of the required active sites [27]. Assessments of reactivity are also hampered by the strong inhibition effects of H_2S products, which cause axial gradients in rates and even in the type of sulfide phase present, even at low reactant conversions.

The chemical nature of catalytic surfaces under relevant conditions (10^{-5}–10^{-2} H_2S/H_2, 573–623 K) has been seldom addressed in these catalytic systems, prompting our investigation of the prevalent phases in HDS catalysts based on Ru and Pt as the active metal at practical HDS conditions [17,18]. These materials exhibit well-known phase boundaries for metal-metal sulfide transformations, which depend on S-chemical potentials and temperature [28]. Ru and Pt catalysts persist as clusters in their metallic state during HDS, consistent with thermodynamic expectations and confirmed by extensive characterization [17,18], thus allowing us to assess turnover rates on such uniform structures. The marked kinetic consequences of a metal or sulfide bulk phase, as shown here for Re-based catalysts that retain their bulk phase during HDS, illustrate how the number of sites that can reversibly bind S-atoms depends critically on the presence of a metal or sulfide core, which must be characterized at sulfur chemical potentials prevalent in HDS catalysis.

Here, we address the site requirements and elementary steps for thiophene HDS reactions on Re-based catalysts, present during reaction in either their metal or sulfide form. Re sulfide, which exhibits a lamellar structure similar to those in Mo and W sulfides, has been reported to show higher HDS rates and hydrogenation selectivities than the Co-MoS_2 compositions widely used in practice [29]. Re metal clusters retained their metallic bulk at practical HDS reaction conditions, thus allowing mechanistic and reactivity studies without any concomitant phase transformations, which would otherwise cause structural changes as S-chemical potentials vary with reaction conditions. Re sulfide structures, formed by sulfidation of Re_2O_7 precursors dispersed on SiO_2 supports, also retained their anisotropic lamellar structure during catalysis. The presence of a different phase when two precursors are exposed to identical conditions reflects significant nucleation barriers in sulfide-metal interconversions during HDS catalysis. This allows the mechanism and reactivity of metal and sulfide Re structures to be compared over a broad range of HDS conditions, without such conditions influencing kinetic responses through phase changes.

Thiophene HDS turnover rates were more than 100-fold higher on ReS_x than on Re metal surfaces at similar S-chemical potentials, set by the prevalent H_2S/H_2 ratios, but all kinetic effects of H_2, thiophene, and H_2S pressures were similar on Re and ReS_x catalysts. They reflect kinetically-relevant addition of H-atoms (H^*) to thiophene (T^*) on interstices within templates of unreactive S-atoms [30], which act as the active site in their vacant form (*). These interstices reversibly bind all reactive intermediates, as required for catalytic turnovers, which must bind S^* and equilibrate it with the contacting H_2S/H_2 mixtures. The different reactivity of Re and ReS_x surfaces thus reflects a different number of interstices on their surfaces, but these interstices exhibit similar binding properties. The larger fraction of these interstices prevalent on ReS_x reflects its weaker M—S bonds relative to those on Re surfaces, and in such an indirect manner M—S bond energies influence HDS turnover rates.

Tetrahydrothiophene (THT) and C_4 (butene/butane) form with THT/C_4 ratios that decrease with residence time but that do not depend on thiophene pressures or S-chemical potentials, indicating that both form as primary products on the same surface sites and that THT can also form C_4 products via readsorption and desulfurization on such sites. The involvement of protonic and hydridic forms of bound H-atoms for these two reactions was previously invoked to account for apparent effects of H_2S in favoring THT products [17,31,32], which are shown here to reflect instead the lower thiophene conversions as H_2S/H_2 ratios increase. Higher H_2 pressures favor THT over C_4 formation via primary routes, showing that C—S cleavage is mediated by transition states that contain fewer H-atoms than for THT formation. These requirements for unsaturated species in C—S cleavage resemble those for C—C cleavage in alkanes and cycloalkanes [33–36] and C—O cleavage in alkanols [37], adding HDS as yet another example of bond scission facilitated by dehydrogenation events, which lead to entropy gains (via H_2(g) formation) and to enthalpic stabilization of C—X (X = C, O, S) cleavage transition states and the weakening of C—X bonds.

2. Methods

2.1. Catalyst synthesis

Supported Re catalysts were prepared using a SiO_2 support (Cabosil, HS-5, 310 m^2 g^{-1}), acid-washed with 1 M HNO_3 and treated in flowing dry air (Praxair, 99.99%, 1.0 cm^3 g^{-1} s^{-1}) at 773 K (0.033 K s^{-1}) for 4 h before contact with Re precursors. Aqueous solutions of NH_4ReO_4 (Aldrich, 99%+) were impregnated onto SiO_2 to the incipient wetness point [38–42], and samples were kept in vacuum at ambient temperature for >12 h and treated overnight in flowing dry air (Praxair, 99.99%, 1.0 cm^3 g^{-1} s^{-1}) at 353 K. Higher Re contents (e.g. 13.5% wt.) required sequential impregnation cycles (because of NH_4ReO_4 solubility) with intervening drying cycles overnight in stagnant air at 353 K [40,41]. Samples were then treated in flowing dry air (Praxair, 99.99%, 1.0 cm^3 g^{-1} s^{-1}) at 573 K (0.033 K s^{-1}) for 3 h, except in the case of the 0.97% wt. sample, which was not treated at 573 K in air before later treatments.

The metal form of these catalysts was prepared by treating the dispersed ReO_x precursors in flowing H_2 (Praxair, 99.999%, 1.0 cm^3 g^{-1} s^{-1}) at 773 K (0.05 K s^{-1}) for 2 h at ambient pressure and then passivating them in O_2/He (Praxair, 0.1% O_2/He, 1.0 cm^3 g^{-1} s^{-1}; ambient temperature, 2 h). Their sulfide form (ReS_x) was prepared by exposing the air-treated samples to flowing H_2S/He (Praxair, 5% H_2S, certified mixture, 45 cm^3 g^{-1} s^{-1}) at 773 K (0.05 K s^{-1}) and ambient pressure for 2 h, after they were loaded into a packed bed reactor. This treatment is denoted as "*in situ* sulfidation" when used before catalytic measurements. Table 1 lists the samples referenced in this study and their respective structural properties.

2.2. Catalyst characterization

Re contents were measured by inductively-coupled plasma optical emission spectroscopy (ICP-OES; Galbraith Laboratories, Inc.). Temperature-programmed reduction (TPR) and X-ray diffraction (XRD; Cu Kα radiation λ = 0.15418 nm, Siemens D500) were carried out on samples after treatment in air. TPR experiments were conducted using 1% H_2/Ar (Praxair, certified mixture, ~90 cm^3 g^{-1} s^{-1}) by heating samples to 1073 K (0.17 K s^{-1}) and measuring H_2 concentrations by thermal conductivity detection (150 mA bridge current) calibrated with a CuO standard.

Transmission electron microscopy (TEM), oxygen chemisorption uptakes, and XRD were used to determine cluster size and metal dispersion. TEM was carried out on samples treated at 773 K (0.05 K s^{-1}) in H_2 (Praxair, 99.999%) or H_2S/He (Praxair, 5% H_2S, certified mixture) flow for 2 h (denoted as fresh samples). These samples were also exposed to a stream with S-chemical potential typical of those prevalent during HDS catalysis (573 K, 3.0 MPa

Table 1
Catalyst dispersion and diameter of Re/SiO_2 and ReS_x/SiO_2.

Nominal/measured weight loading (% wt. Re)	Phase	Re dispersion[b]	Cluster diameter (nm)	Dispersity Index (DI)[f]
15/13.5[a]	Re^0	0.17	6.9[d]/6.9[e]	1.3
15/13.5[a]	ReS_x	1[c]	–	–
5/4.3[a]	Re^0	0.41	2.9[d]/2.4[e]	1.2
5/4.3[a]	ReS_x	1[c]	–	–
1/0.97[a]	Re^0	0.95	1.2[d]/–	–

[a] Measured from ICP-OES elemental analysis (Galbraith Laboratories, Inc.).
[b] Based on O_2-chemisorption assuming a O:Re_s stoichiometry of 0.4:1 (see Section 3.1).
[c] Sulfide phases are assumed to be fully-dispersed.
[d] Calculated from Re dispersion, assuming spherical clusters and bulk diameter of Re metal: < diameter > (nm) = 1.18/(fractional dispersion).
[e] Surface-averaged diameter from cluster size distributions measured via TEM (Eq. (1)).
[f] Calculated from the ratio of surface-averaged to number-averaged cluster sizes (Eq. (2)).

H_2, 1.0 kPa H_2S; 5 h), cooled in He (Praxair, 99.999%) flow, and passivated with O_2/He (Praxair, 0.5% O_2/He, certified mixture) in order to assess any structural changes caused by exposure to the S-chemical potentials relevant in HDS catalysis (denoted as spent samples). TEM samples (fresh and spent) were prepared by dispersing powders in acetone and placing the suspension dropwise onto an ultrathin holey carbon film supported on a 400 mesh copper grid (Ted Pella, Inc.). The deposited samples were dried at ambient conditions and examined using a JEOL 1200 EX TEM operated at 80 kV or a Philips 420 TEM operated at 120 kV. Surface-averaged cluster sizes were calculated from > 300 Re particles using the equation:

$$\langle d\rangle_{surf} = \frac{\sum_i n_i d_i^3}{\sum_i n_i d_i^2} \tag{1}$$

where n_i represents the frequency of clusters exhibiting a diameter of d_i.

The dispersity index (DI) was calculated by normalizing the surface-averaged diameter by its number-averaged diameter:

$$DI = \frac{\langle d\rangle_{surf}}{\langle d\rangle_{number}};\ \langle d\rangle_{number} = \frac{\Sigma_i n_i d_i}{\Sigma_i n_i} \tag{2}$$

with values below 1.5 typical of monodispersed, colloidal metal clusters [43].

O_2 chemisorption uptakes were measured volumetrically on Re/SiO_2, following similar protocols reported in the literature [24–26], at 0.1–50 kPa O_2 pressure (Praxair, 99.999%) and 298 K, 323 K, and 473 K, after treating passivated samples in pure H_2 flow (Praxair, 99.999%, 17 $cm^3\ g^{-1}\ s^{-1}$) at 773 K (0.05 K s^{-1}) for 1 h and evacuating (1 Pa typical) while cooling to ambient temperature over 2 h (Pfeiffer Vacuum IPS 100). Re dispersions (defined as the fraction of Re atoms exposed at cluster surfaces relative to total Re atoms, Re_{surf}/Re_{total}) were determined using a 0.4:1 O:Re_s stoichiometry (determined by TEM comparisons, Section 3.2). Volume-averaged cluster diameters were obtained from Rietveld refinement analysis (Maud software [44]; SI, S.1) of diffractograms obtained from XRD.

The formation of H_2S during H_2 treatment of samples treated in H_2 or H_2S/He (fresh samples) and of samples treated under simulated HDS conditions (spent samples) was used to determine S/Re ratios; these experiments are denoted as TPR-S in order to distinguish them from H_2 treatments intended to remove O-atoms from ReO_x precursors. Fresh samples, after their treatments in H_2 and H_2S/He (as described in Section 2.1), were cooled in flowing He to ambient temperature before TPR-S experiments. Spent samples, after exposure to typical HDS temperatures and S-chemical potentials (573 K, 3.0 MPa H_2, 3.0 kPa H_2S; 3 h), were also cooled in flowing He to ambient temperature before TPR-S. All samples (0.015 g) were then exposed to a H_2-containing stream (2% H_2/8% Ar/He mixture, Praxair, certified mixture, 220 $cm^3\ g^{-1}\ s^{-1}$) and heated to 873 K or 973 K (0.17 K s^{-1}) and held at that temperature for 1 h. The H_2S formed during the experiment was detected by mass spectroscopy (Leybold Inficon, Transpector Series; response factors from H_2S calibration standards) in order to determine S/Re ratios in each sample.

Fresh and spent samples (prepared by the same treatments described above for TEM analysis) of 4.3% wt. ReS_x/SiO_2 and Re/SiO_2 (0.41 dispersion, Table 1) were also examined using X-ray absorption spectroscopy (XAS). After cooling to ambient temperatures in He, samples were rapidly transferred in a N_2 atmosphere into a XAS cell. The Re L_{III}-edge was used to obtain the X-ray absorption near-edge structure (XANES) and the extended X-ray absorption fine structure (EXAFS) spectra at the Stanford Synchrotron Research Laboratory (SSRL, Beamline 4-1). EXAFS data were extracted from the raw files using the Athena software; the regression of structural parameters was carried out using the Artemis software [45,46] over the k-range (photoelectron wave number) and absorber-scatterer distances of 3.5–16.1 Å^{-1} and 1.5–5.7 Å, respectively, for Re/SiO_2 [47,48] and 2.0–15.9 Å^{-1} and 1.0–3.5 Å [47,48], respectively, for ReS_x/SiO_2 [47,48]. Transmitted and incident X-ray intensities (I_t and I_0) were used to calculate absorption coefficients (μ) as a function of incident energies (E). Background subtraction and normalization of μ by the step height change at the absorption edge energy ($\Delta\mu_0$) gave χ(E), defined as:

$$\chi(E) = \frac{\mu(E) - \mu_0(E)}{\Delta\mu_0} \tag{3}$$

where μ(E) is the measured absorption coefficient and μ_0(E) is the fitted absorption coefficient reflecting the absorption of an isolated atom. This function can be regressed to the form of the EXAFS equation [49,50], which describes constructive and destructive interference patterns from emitted photoelectron scattering, by using single and multiple scattering pathway models (FEFF program [51]) in order to derive structural parameters such as absorber-scatterer coordination numbers and distances.

2.3. Hydrodesulfurization rates and selectivities

Turnover rates and product selectivities were measured in a packed bed reactor with plug-flow hydrodynamics [17,18]. Re/SiO_2 samples were diluted with SiO_2 (Cab-O-Sil, HS-5, 310 $m^2\ g^{-1}$) at 1:1 and 4:1 diluent:catalyst ratios (by mass). ReS_x/SiO_2 samples were prepared by treating ReO_x/SiO_2 samples in H_2S/He in the reactor prior to catalytic measurements (*in situ* sulfidation), and thus, the air-treated powder precursors were loaded into the reactor either in undiluted form or diluted 1:1 with SiO_2 (Cab-O-Sil). For diluted mixtures, the samples were pressed and sieved to retain 0.125- to 0.180-mm aggregates. Aggregates were mixed with quartz granules of similar size in order to ensure isothermal reactors. Calculations using the Mears' criterion for internal transport artifacts confirmed the absence of any mass or heat transfer effects on measured rates [52] (SI, S.2).

After samples were loaded into the reactor, they were exposed to treatments in pure H_2 (Praxair, 99.999%, 2.9 $cm^3\ g^{-1}\ s^{-1}$) or 5% H_2S/He (Praxair, certified mixture, 45 $cm^3\ g^{-1}\ s^{-1}$) at 773 K for 2 h within the reactor in order to form Re/SiO_2 or ReS_x/SiO_2, respectively (Section 2.1). Temperatures were then decreased to 573 K, and H_2 (Praxair, 99.999%) and H_2S (0.5% H_2S/H_2, Praxair, certified mixture) pressures were set to the desired values. Thiophene (Alfa Aesar, 99%) and decane (Aldrich, 99+%, used as the thiophene solvent and internal standard) were vaporized into the H_2S/H_2 flow using a high-pressure syringe pump (Isco 500D); the injection point and all transfer lines thereafter were kept above 433 K to avoid condensation.

The speciation and concentrations of all compounds in the effluent stream were determined by on-line gas chromatography (Agilent 6890) using a methyl silicone capillary column (HP-1, Agilent, 25 m × 0.32 mm × 0.52 μm film) connected to a flame ionization detector and a Porapak Q packed column (Supelco, 1.82 m × 3.18 mm, 80–100 mesh) connected to a thermal conductivity detector. Rates are reported as the molar rate of conversion of thiophene normalized per surface g-atom for Re catalyst from oxygen chemisorption and per total Re atom for ReS_x (because their small lamellar structures did not allow accurate dispersion estimates), thus providing a lower bound for reactivity of the latter. Residence times and concentrations were varied by changing H_2, H_2S, and thiophene flow rates using electronic controllers (Parker, Series 201); system pressures were maintained using a back pressure regulator (Mity Mite) with a Teflon diaphragm (Freudenberg Oil and Gas). Axial concentration and chemical potential gradients were minimized by co-feeding H_2S, maintaining low conversions (3–15%), and extrapolating data to zero residence time where required. Rates were measured over a broad and practical range of H_2 (1–3 MPa), H_2S (0.2–3.0 kPa), and thiophene (1–10 kPa) pressures.

3. Results and discussions

3.1. Structure of Re-based catalysts and effects of treatment protocols

X-Ray diffractograms showed lines corresponding to Re_2O_7 crystallites after impregnation and treatment in air at 573 K (SI, S.3, Fig. S.3-1), consistent with the reported Re-ReO_x-O_2 phase diagram [53]; these diffraction lines were very broad, thus preventing reliable estimates of the mean cluster diameters of these ReO_x precursors, but indicative of highly dispersed Re_2O_7 domains. These

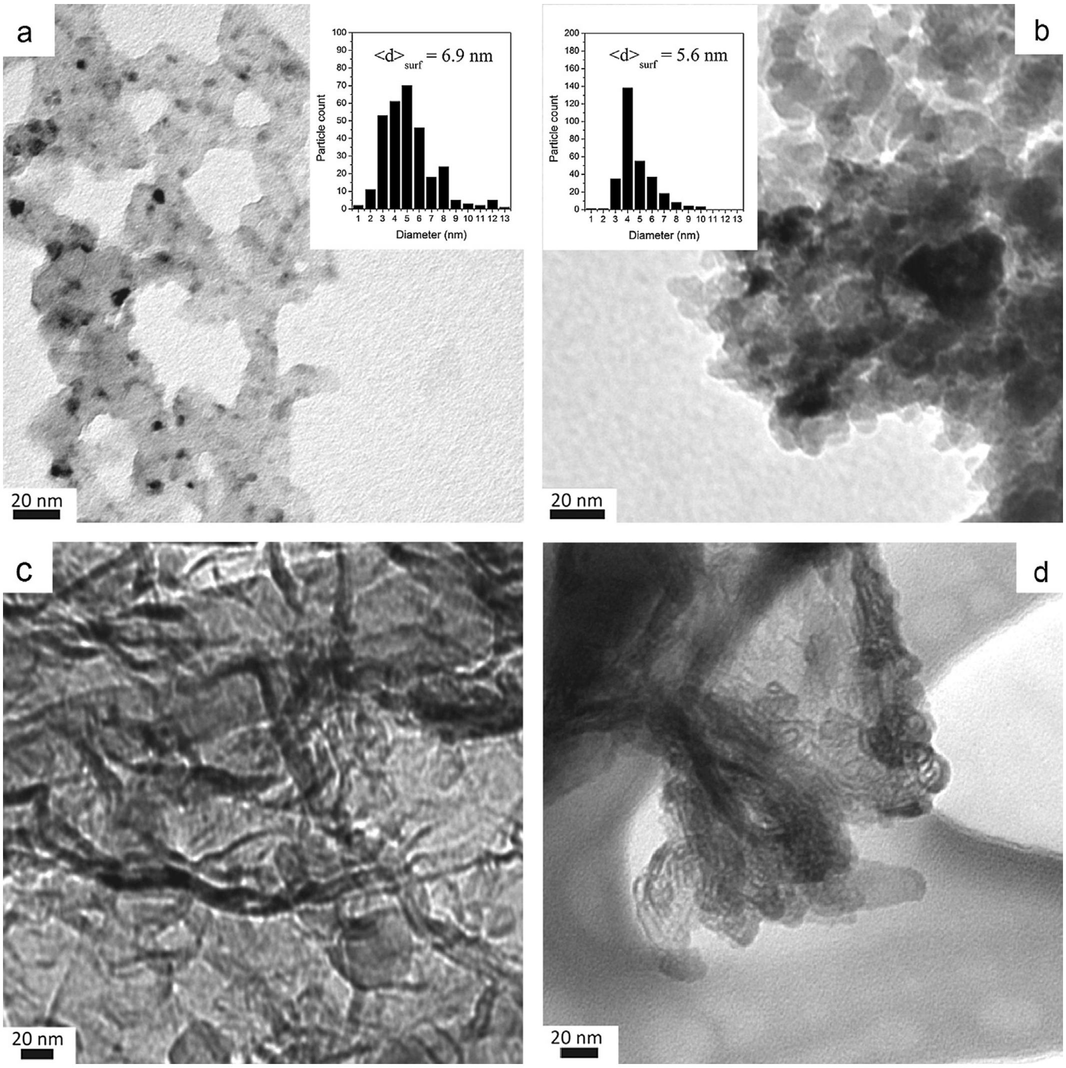

Fig. 1. TEM images of (13.5% wt.) of Re/SiO_2 (a) after H_2 treatment of ReO_x at 773 K and (b) after exposure to simulated hydrodesulfurization conditions (3.0 MPa H_2, 0.00033 H_2S/H_2, 573 K) and of ReS_x/SiO_2 (c) after H_2S/He treatment of ReO_x at 773 K and (d) after exposure to simulated hydrodesulfurization conditions (3.0 MPa H_2, 0.00033 H_2S/H_2, 573 K).

ReO_x precursors formed Re metal clusters after thermal treatment in H_2 and ReS_x domains after treatment in H_2S/He mixtures (Section 2.1). The sharp H_2 consumption peaks observed below 770 K reflect the autocatalytic reduction of Re^{7+} to Re^0 [41,54,55] (SI, S.4, Fig. S.4-1); the amount of H_2 consumed ($H_2/Re = 3.4–3.6$) is consistent with the reduction of Re_2O_7 to Re^0. TEM images showed very different morphologies after treatment in H_2 and H_2S/He at 773 K. H_2-treated samples showed quasi-spherical Re clusters (Fig. 1a) while samples exposed to H_2S gave the lamellar structures (Fig. 1c) characteristic of ReS_x [29].

The radial structure functions of Re/SiO_2 (Fig. 2a; 4.3% wt. loading, 2.4 nm TEM surface averaged diameter) exhibited features similar to those for a Re foil standard and to those reported elsewhere for Re metal particles (on mordenite/γ-Al_2O_3 mixed support) treated in moist H_2 at 773 K [48]; the radial structure functions, however, exhibited weaker features for Re/SiO_2 than for Re foils, as expected from the smaller number of neighboring scatterers and the lower Re-Re coordination numbers in small clusters. The formation of ReS_2 upon treatment of ReO_x/SiO_2 samples in H_2S/He at 773 K is evident from the lamellar features in micrographs (Fig. 1c), from the S/Re ratio of 2.05 during H_2 treatments (Fig. 3a; TPR-S), and from a radial structure function (Fig. 2b) that resembles that for a bulk ReS_2 standard [47]. The structure and S-content of these Re/SiO_2 and ReS_2/SiO_2 samples after exposure to a stream with S-chemical potentials typical of HDS catalysis ($H_2S/H_2 = 3.3 \times 10^{-4}$, 573 K) were also examined. TEM images showed that ReS_x lamella remained intact (Fig. 1d), in spite of the loss of S-atoms (S/Re = 1.32 vs. 2.05; Fig. 3b). Re^0 clusters did not change appreciably in structure or size (6.9 vs. 5.6 nm after H_2S/H_2 treatment; 13.5% wt. Re/SiO_2; Fig. 1a and b) upon exposure to H_2S/H_2 mixtures; their low S/Re ratio (0.10; Fig. 3c) corresponds to about 0.6 ML S^* on Re^0 clusters with 0.17 dispersion (Table 1).

Radial structure functions for the fresh Re/SiO_2 and the ReS_x/SiO_2 samples were very different, but each remained unchanged after contact with H_2S/H_2 mixtures (Fig. 2). X-Ray absorption data were regressed to the EXAFS equation [49,50]; the resulting fits, using models that considered only the first coordination sphere for ReS_x and up to the third shell for Re, allowed estimates of coordination numbers, bond lengths, and Debye-Waller factors for relevant scattering paths using established procedures [45,46] and the atomic positions in the bulk crystal structures of Re and ReS_x as the initial structure in optimizations [47,48]. Coordination numbers and bond lengths (Re-Re, Re-S) were consistent with previous EXAFS studies [47,48] on bulk ReS_x and Re nanoparticles (~3 nm cluster size).

A L_{III} Re-S first-shell single scattering path was included in the Re/SiO_2 structure refinement (Fig. 2c) in order to determine whether bound S-atoms were detectable at Re metal surfaces exposed to H_2S/H_2 ratios prevalent during HDS catalysis. The Re-S distance (0.236 nm), determined from regression of the fine structure of this sample, was slightly shorter than in ReS_x after sulfidation and also after exposure to H_2S/H_2 (0.238 nm), consistent with the stronger (and shorter) Re-S bonds expected at Re metal surfaces compared to Re-S bonds in bulk ReS_2 [30,56]. Re-Re

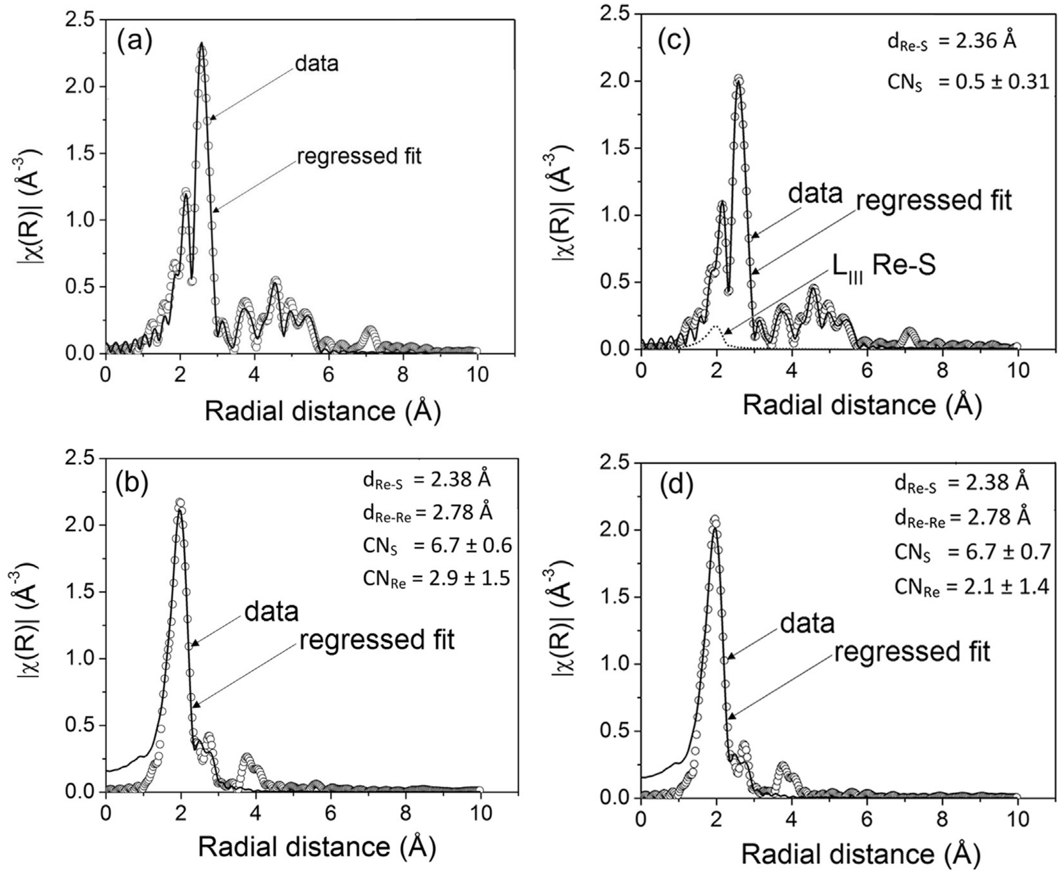

Fig. 2. Fourier transforms for the EXAFS spectra (corrected by phase shift) for (4.3% wt.) (a) fresh Re/SiO_2 and (b) fresh ReS_x/SiO_2, synthesized from ReO_x and for (c) spent Re/SiO_2 and (d) spent ReS_x/SiO_2, after exposure to simulated hydrodesulfurization conditions (3.0 MPa H_2, 1 kPa H_2S, 573 K). Spectral fits were based on the EXAFS equation, χ(R) [48], over range of k (photoelectron wave number) and R (distance between absorbing and scattering atoms) of 3.5–16.1 Å^{-1} and 1.5–5.7 Å, respectively, for Re/SiO_2 and of 2.0–15.9 Å^{-1} and 1.0–3.5 Å, respectively, for ReS_x/SiO_2. Multiple (Re) or single (ReS_x) photoelectron scattering pathway models are used to fit (—) measured spectra (○). The regression indicated as a dotted line (···) represents the inclusion of an additional Re-S scattering path for the spent Re/SiO_2 (c). The distances (d_{Re-Re}, d_{Re-S}) reflect the bond length of the absorber-scatterer pair (Re-Re and Re-S, respectively) and CN_i denotes the number of nearest i neighbors (coordination number) in the first shell.

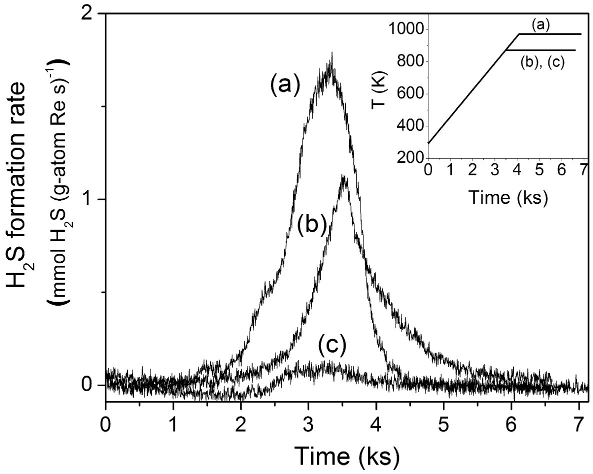

Fig. 3. Temperature programmed reduction (TPR-S) profiles shown as H_2S formation rates and used to determine the S-content of (13.5% wt.) (a) fresh ReS_x/SiO_2, (b) spent ReS_x/SiO_2 (after exposure to simulated hydrodesulfurization conditions: 3.0 MPa H_2, 0.001 H_2S/H_2, 573 K) and of (c) spent Re/SiO_2 (after exposure to simulated hydrodesulfurization conditions: 3.0 MPa H_2, 0.001 H_2S/H_2, 573 K). Inset: temperature ramp used for all samples.

features in the Re/SiO_2 sample, however, overlapped those for Re-S, and measured spectra were well-described whether this Re-S scattering path was included or not. Consequently, the presence of chemisorbed S-atoms on Re/SiO_2 after H_2S/H_2 treatments cannot be determined unequivocally from this analysis but is clearly evident from S/Re ratios (Fig. 3c). ReS_x/SiO_2 gave nearly identical X-ray absorption spectra before and after H_2S/H_2 treatment, even though they contain different S/Re ratios (2.05 and 1.32), indicative of negligible changes to the bulk structure of ReS_x.

The near-edge region in EXAFS spectra showed a white-line at the L_{III} Re edge (Fig. 4), corresponding to the excitation of 2p electrons to 5d bound states; its intensity is expected to increase as the 5d occupancy decreases upon oxidation of Re centers. The formal oxidation state of Re should increase as its surface is titrated by S-adatoms upon exposure of Re/SiO_2 to H_2S/H_2 mixtures. Instead, the white-line weakened upon exposure of Re/SiO_2 to H_2S/H_2, suggesting that Re did not oxidize as Re-S bonds were formed. This observation suggests that sulfur is a weaker oxidant than oxygen; indeed, sulfur is less electronegative than oxygen, and M—S bonds in transition metal sulfides are known to be more covalent than M—O bonds in transition metal oxides [57,58]. Some studies have also suggested that chemisorption of sulfur compounds on transition metal surfaces occurs via electron donation from the S-atom to the d-orbitals of the metal [59], which would lead, as observed here, to a decrease in white-line intensity upon formation of S-adlayers. Indeed, slightly weaker white-line features were observed for ReS_x/SiO_2 relative to Re/SiO_2 (for samples not exposed to H_2S/H_2), which seems consistent with electron donation from S-atoms to Re centers, in spite of the Re^{4+} formal valence in ReS_2. As evident from the difference spectrum ($\Delta\mu$) of the fresh and spent ReS_x (Fig. 4, inset, ii), ReS_x/SiO_2 samples gave stronger white-line features after exposure to H_2S/H_2 mixtures, a treatment that led to the loss of S-atoms, as shown by TPR-S (Fig. 3). The XANES features in Re and ReS_x retained their significant differences after exposure to HDS-type conditions (Fig. 4, inset, iii), indicating that exposure to similar H_2S/H_2 ratios for 5 h, in contrast with the behavior of Ru and Pt catalysts [17,18], did not lead to similar structures and oxidation states. Overall, these trends indicate an increase in valence electron density around the Re center with increasing number of Re-S bonds, in spite of the oxidation state formalisms typically cited.

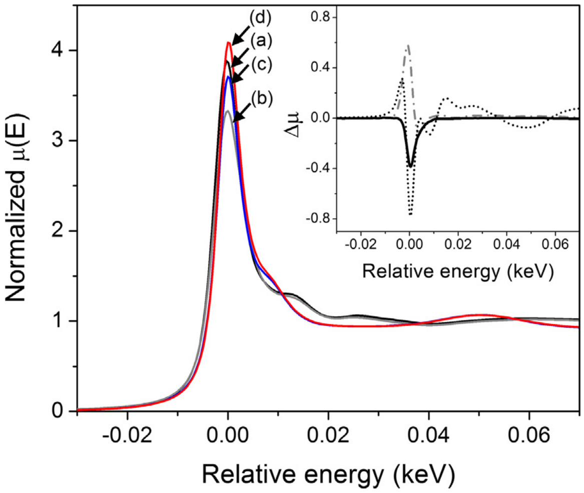

Fig. 4. Normalized XAS absorption coefficient (μ), measured from ratios of incident (I_o) and transmitted (I_t) X-ray intensities ($I_t = I_0e^{-\mu x}$, x is sample thickness) as a function of relative energy, referenced to the edge energy measured on Re foil at SSRL (10.54 keV), for (4.3% wt.) Re/SiO_2 (a) after H_2 treatment of ReO_x at 773 K (fresh Re) and (b) after exposure to simulated hydrodesulfurization conditions (3.0 MPa H_2, 0.00033 H_2S/H_2, 573 K) (spent Re) and for ReS_x/SiO_2 (c) after H_2S/He treatment ReO_x at 773 K (fresh ReS_x) and (d) after exposure to simulated hydrodesulfurization conditions (3.0 MPa H_2, 0.00033 H_2S/H_2, 573 K) (spent ReS_x). Inset: differences in μ near the L_{III} edge of (i) $\mu_{fresh\ Re} - \mu_{spent\ Re}$ (- -), (ii) $\mu_{fresh\ ReSx} - \mu_{spent\ ReSx}$ (—), and (iii) $\mu_{spent\ Re} - \mu_{spent\ ReSx}$ (···).

The metastable nature of the structures formed by the initial treatments of Re_2O_7/SiO_2 precursors is consistent with measured HDS rates and selectivities (at 3.0 MPa H_2, 2.5 kPa thiophene, 573 K) on Re/SiO_2 and ReS_x/SiO_2 that remained constant with time for more than 100 h (Fig. 5), indicative of their unchanged respective structures during catalysis. Turnover rates were, however, about 100-fold larger on ReS_x/SiO_2 than Re/SiO_2; this represents a lower bound for the turnover rate on ReS_x because all Re atoms in this sample are assumed to reside at surfaces (Section 3.2). Thermodynamic data from Re-S phase diagrams [28] show that bulk Re metal is the stable phase at all reaction conditions (<0.01 H_2S/H_2, 573 K). It seems plausible that nucleation barriers prevent the significant structural rearrangements required to interconvert lamellar structures of ReS_2 and isotropic hcp structures of Re metal at these temperatures. Turnover rates on a ReS_x/SiO_2 sample, subsequently treated in H_2 at the conditions used to form Re/SiO_2 from Re_2O_7/SiO_2 (Section 2.1), were lower than those on fresh ReS_x/SiO_2 (SI, S.5, Fig. S.5-1; 1.9×10^{-2} to 0.41×10^{-2} s^{-1} after treatment in H_2, 773 K, 2 h), indicative of the conversion of some ReS_x to Re metal at these higher temperatures, as expected from the evolution of some H_2S from ReS_x at 773 K during TPR-S (Fig. 3a). A subsequent sulfidation treatment (5% H_2S/He, 773 K, 2 h), however, did not restore initial rates for this sample, consistent with the refractory nature of Re metal towards the nucleation of the thermodynamically stable ReS_x phase, even at these high sulfur chemical potentials. These interconversion hurdles are apparently much less severe for the conversion of ReO_x to Re or ReS_x.

3.2. Dispersion of Re^0 and ReS_x structures

H_2 chemisorption methods are widely used to measure metal dispersions [17,18] but are unreliable for Re-based materials because H_2 dissociation barriers lead to inconsistent $H:Re_s$ ratios at saturation [24,39,60–62]; such adsorption stoichiometries are also unreliable for CO and O_2 titrants [24] because of diverse bound configurations and subsurface penetration, respectively. The oxophilic nature of Re atoms leads to O^* saturation coverages at

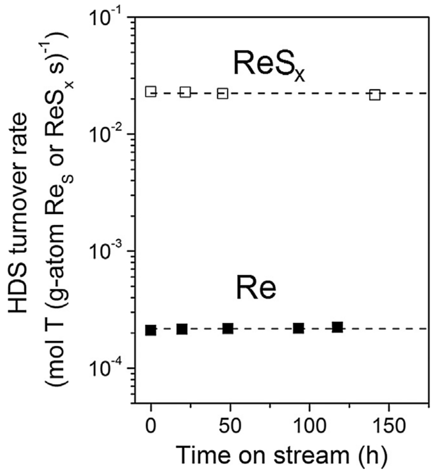

Fig. 5. Hydrodesulfurization turnover rates of thiophene (T) consumption on (13.5% wt.) Re/SiO_2 (■) and ReS_x/SiO_2 (☐) normalized by surface and total moles of Re, respectively, as a function of time on stream (3.0 MPa H_2, 2.5 kPa thiophene, 573 K, 15–20% conversion).

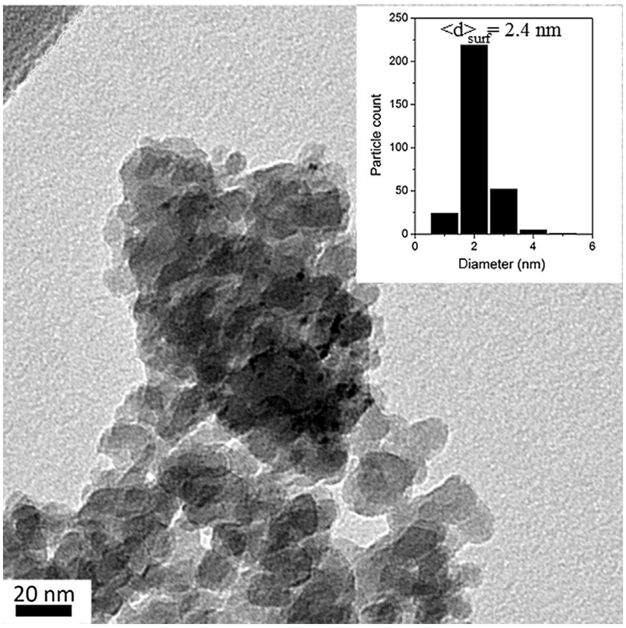

Fig. 6. Transmission electron micrograph and measured particle diameter distribution for 4.3% wt. Re/SiO_2, after H_2 treatment of Re_2O_7 at 773 K for 2 h using the procedure described in Section 2.1. Surface-averaged particle size (<d>$_{surf}$), from TEM, is reported.

near ambient temperatures, thus inhibiting its diffusion into the bulk. The broad range of reported saturation O/Re_s stoichiometries (0.50–1.0 ML [24–26]) required that we confirm a more reliable value by comparing TEM and adsorption data on 4.3% and 13.5% wt. Re/SiO_2, which contain large numbers of TEM-detectable and nearly monodispersed clusters (Figs. 6 and 1a; dispersity indices of 1.2–1.3) with 2.4 nm and 6.9 nm mean diameters, respectively. Such comparisons gave similar saturation coverages on both samples at 323 K (0.34 and 0.41 ML O^*). These uptakes were similar at 298 K and 323 K, but increased at 373 K, indicative of the onset of bulk diffusion (SI, S.6, Fig. S.6-1). The dispersion of the 0.97% wt. Re/SiO_2 sample could not be measured from micrographs; it was determined to be 0.95 from O_2 uptakes (using 0.4 ML O^* as saturation), corresponding to a mean particle size of about 1 nm.

Rietveld refinement of X-ray diffractograms for 13.5% wt. Re/SiO_2 (SI, S.1, Fig. S.1-1) gave a (volume-averaged) mean diameter larger than that from TEM size distributions (13 vs. 7.3 nm). These differences may reflect the presence of a few large Re crystallites that are difficult to distinguish from support agglomerates in micrographs, but which contribute disproportionately as sharp and intense components of the diffraction lines.

The surface area of ReS_x lamellae could not be accurately determined from micrographs or chemisorption uptakes. Methods that count active sites from the length and stacking number of sulfide layers require assumptions about their trigonal or hexagonal arrangements in reconstructing the two-dimensional TEM projections [19]; these methods assume that only edge sites in these lamellar structures (e.g. MoS_2) are active for HDS. O_2 uptakes on sulfides merely reflect the number of vacancies formed by a given reductive treatment and act as reactivity predictors for a given composition [13]; they cannot be used, however, as site counts in determining turnover rates [63]. Consequently, turnover rates reported here are based on the assumption that all Re atoms in ReS_x are present at surfaces, consistent with the well-dispersed lamellar structures evident from TEM images. These turnover rates, for both Re and ReS_x, reflect measured rates, normalized on a consistent basis of exposed atoms, without designating which of these exposed atoms participate in turnovers as "active sites." Instead, we infer the nature of the working surfaces from how these rates vary with the structure of the domains that contain these sites, rather than presupposing, for instance, the involvement of specific "hydrogenation sites" or of certain charged H-species ($H^{\delta+}$, $H^{\delta-}$), assigned without convincing evidence to rim or edge regions of layered structures in the case of MoS_2 [6,27,64]. In fact, the involvement of such distinct sites would contradict our data, which indicate that all products (i.e., tetrahydrothiophene, butene, and butane) form on similar types of sites (Section 3.3) and that both Re and ReS_x exhibit similar kinetic trends and selectivities (Sections 3.4 and 3.5). These observations support the argument that HDS can occur, as in the case of most redox cycles on oxides, on basal planes with labile heteroatoms.

3.3. Thiophene hydrodesulfurization turnover rates on Re/SiO_2 and ReS_x/SiO_2 catalysts

The depletion of thiophene reactant and the concomitant formation of H_2S cause rates to decrease with increasing residence time (Fig. 7). H_2S added to H_2/thiophene reactants maintained a nearly constant axial S-chemical potential along the bed; such reactant mixtures, together with modest thiophene conversions (5–10%), imposed nearly differential conditions, thus allowing rates and selectivity measurements with modest or no extrapolation to the condition at the reactor inlet. Thiophene forms an organosulfur compound (tetrahydrothiophene; THT) and acyclic alkenes and alkane (1-butene, *cis*-2-butene, *trans*-2-butene, *n*-butane; C_4) (Fig. 8). Neither butadiene nor dihydrothiophene were evident in the effluent (dihydrothiophene traces were detected in ReS_x), in contrast with their presence among thiophene products on Ru and Pt catalysts [17,18]; the facile hydrogenation steps indicated by such products are also evident in the prevalence of butane among C_4 products. All linear butene regioisomers were equilibrated and are treated here as one lumped product. No hydrogenolysis products of the n-decane internal standard used were detected.

Primary THT products also form linear C_4 products via secondary reactions on Re and ReS_x at all H_2 pressures (1–3 MPa) (Scheme 1), leading to lower THT selectivity and higher C_4 selectivities with increasing residence time (Fig. 8). The selectivity to primary products (those formed during a single surface sojourn) is given by extrapolation to zero conversion using the functional

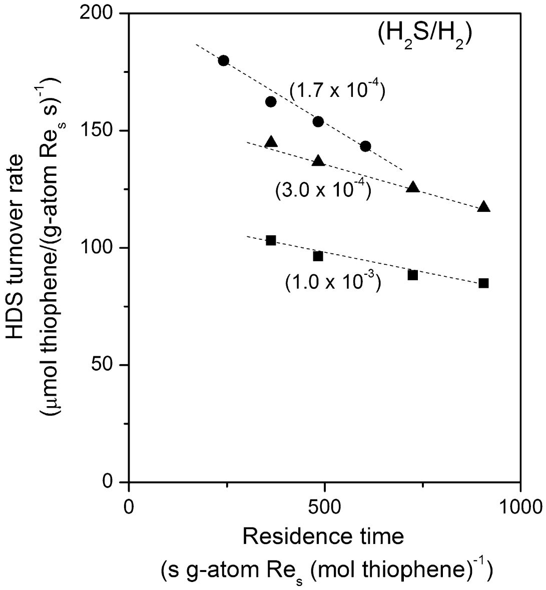

Fig. 7. Hydrodesulfurization turnover rates of thiophene consumption as a function of residence time for different H_2S/H_2 ratios (1.7×10^{-4} (●), 3.0×10^{-4} (▲), 1.0×10^{-3} (■)) on 13.5% wt. Re/SiO$_2$ (3.0 MPa H_2, 2.5 kPa thiophene, 573 K). Dashed lines indicate trends.

form of a mechanism-based rate equation (Section 3.5). Thiophene conversion rates depend sensitively on thiophene pressure and H_2S/H_2 ratio (Fig. 9a and c), but selectivities and their trends with conversion are unaffected over a nearly ten-fold range of these pressures and ratios (Fig. 8), indicating that the pathways that form THT and C_4 occur on sites that sense adsorbed species derived from reactants and products to an identical extent.

H_2S inhibits HDS rates [2,4,5,65], leading some previous studies to infer that it also favors THT over C_4 products [17,31,32] and to propose that $H^{\delta+}$ species, formed via heterolytic H_2S dissociation on M—S site pairs (*—*S) to give ($^*S^{\delta-}H^{\delta+}$—$^*S^{\delta-}H^{\delta+}$) species [66,67], mediate the hydrogenation routes. The data in Figs. 8 and S.7-1 show that such pathways are not required to account for the effects of H_2S on THT/C_4 ratios, and previous reports of such effects merely reflect inaccuracies in the extrapolations to zero conversion. In fact, THT and C_4 selectivities, and thus their ratios, were unaffected by H_2S/H_2 ratios over a ten-fold range when these selectivity ratios are compared at the same thiophene conversion (Fig. 8).

3.4. Elementary steps of thiophene hydrodesulfurization on Re and ReS$_x$ catalysts

Traces of H_2S and organosulfur compounds (<1 ppm) strongly inhibit (de)hydrogenation, hydrogenolysis [59], reforming [30], and Fischer-Tropsch synthesis [68] on metals via the formation of dense S-adlayers, which is also evident from the adsorption of S-atoms on low index extended metal (Ni, Pt, Re) surfaces [69–71]. Such dense adlayers reflect large and negative S-adsorption enthalpies (at $\leq$0.50 saturation coverage, -100 to -150 kJ (mol $H_2S)^{-1}$) on supported metal clusters (Ni, Ru, Fe, Co, Pt, Ir) [72–76].

Equilibrated dissociation of H_2S onto metal sites (M) leads to bound H* and S*. When H_2 dissociation is also equilibrated, surface coverages and S-chemical potentials depend solely on H_2S/H_2 ratios:

$$M(s) + H_2S(g) \leftrightarrow M-S(surface) + H_2(g); \quad \Delta G^0_{ads} = RT\ \ln(P_{H_2S}/P_{H_2}) \tag{4}$$

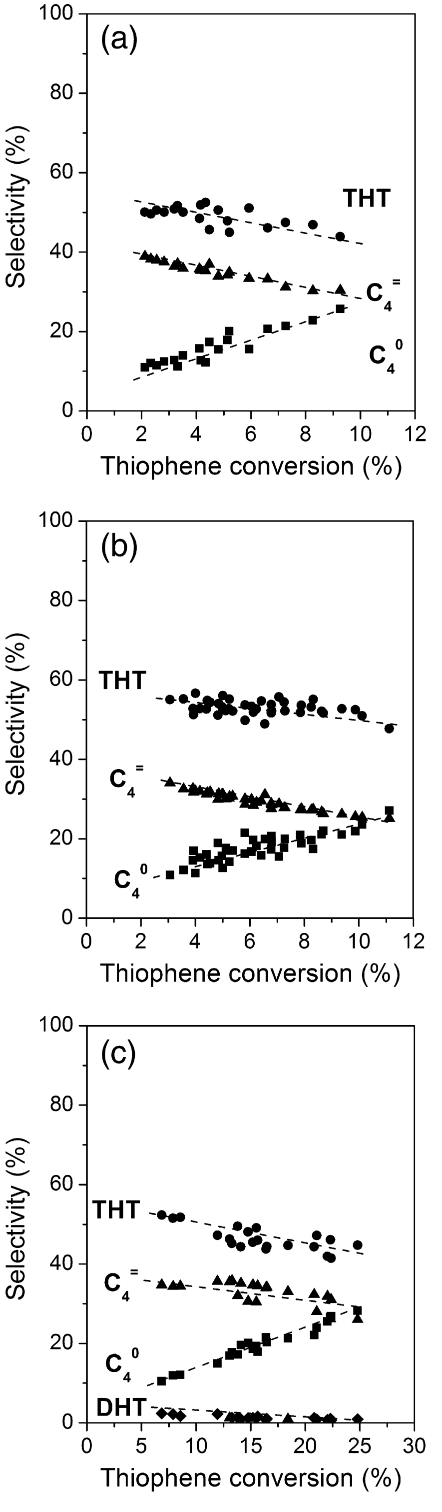

Fig. 8. Selectivity to tetrahydrothiophene (THT, ●), linear butenes ($C_4^=$, ▲), n-butane (C_4^0, ■), and dihydrothiophene (DHT, ◆) as a function of conversion on 13.5% wt. Re/SiO$_2$ at (a) 2.0 MPa H_2, (b) 3.0 MPa H_2 and on 13.5% wt. ReS$_x$/SiO$_2$ at (c) 3.0 MPa H_2 at 573 K, 1.0–10 kPa thiophene pressures and (0.67–5) $\times 10^{-4}$ H_2S/H_2 ratios.

H_2S/H_2 ratios present during HDS catalysis are much higher than those required to form saturated adlayers (>10^{-5}) at typical reaction temperatures (573–673 K). The consequent high density of S-atoms at surfaces leads to a dearth of vacant sites, which are required as intermediates during catalytic turnovers, thus causing a strong decrease in rates as H_2S/H_2 ratios increase (Fig. 9c). In

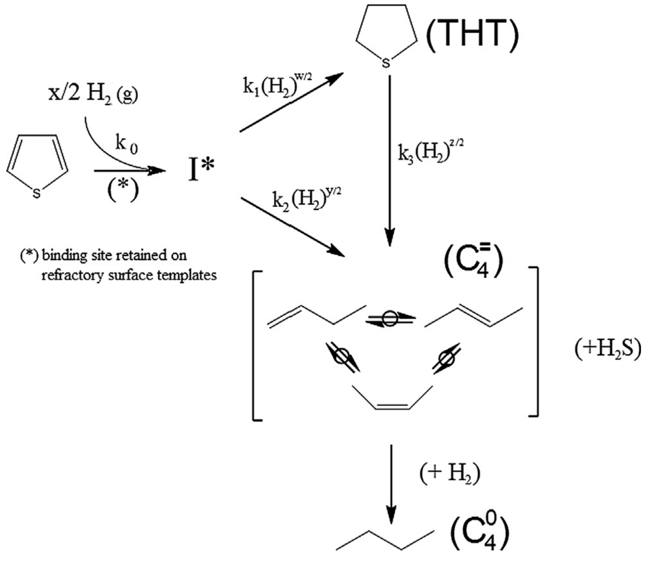

Scheme 1. Proposed network for thiophene reaction on active surface templates of Re and ReS_x. Thiophene and H_2-derived species adsorb on interstitial binding sites (*), retained on refractory surface templates of S-adatoms. Thiophene consumption rates are mediated by a kinetically-relevant transition state derived from thiophene and *x* H-atoms (*x* = 1, 2, 3, or 4) to form a common reaction intermediate, I^*. Tetrahydrothiophene (THT) and butene ($C_4^=$) are observed primary products on Re and ReS_x, and they form from subsequent surface reactions of I^* and H-atoms on similar types of sites. The kinetically-relevant transition states that mediate THT and $C_4^=$ formations are derived from I^* and *w* and *y* H-atoms, respectively. Secondary THT desulfurization reactions to form $C_4^=$ also occur. All linear butene regioisomers are equilibrated and form butane (C_4^0) via secondary hydrogenation reactions.

some instances, high H_2S/H_2 ratios can also lead to the formation of their respective sulfide phase, when nucleation barriers are sufficiently small to allow the system to reach the phase dictated by thermodynamics.

HDS rates increased with increasing H_2 and thiophene pressures (Fig. 9a and b), indicating that the transition state that mediates the kinetically-relevant step contains a thiophene-derived species with added H-atoms. Their sublinear dependencies on thiophene pressure are unexpected on S-saturated surfaces, for which kinetic treatments would lead to integer kinetic orders; these trends indicate that thiophene-derived (and possibly H_2-derived) species, in addition to those formed from H_2S, influence the denominator terms in the rate equation. This suggests, in turn, the competitive adsorption of species derived from thiophene and H_2S, in spite of the expected strong binding and saturated coverages of S^* even at much lower S-chemical potentials than those prevalent in HDS practice. This also implies that HDS turnovers must occur on refractory surface "templates" of S-adatoms that are able to retain interstitial spaces and thus bind all reactive intermediates in the reversible manner required for catalytic turnovers. These interstitial spaces become then the vacant binding sites, and they define the working surface in its uncovered state, thus retaining the Langmuirian properties required for the accepted treatments of chemical kinetics on uniform surfaces.

The involvement of these interstices within S-adlayers as active centers merely reflects the well-established repulsive interactions that lead to ordering in adlayers and to S-binding energies that decrease with increasing coverage [72–76], frequently in an abrupt and stepwise manner with S^* coverage and with a frequent sharp drop in binding energies specifically at ~0.8 ML. Similarly, extended flat surfaces [69–71] saturate at 0.5–0.6 ML and form ordered structures that maximize S-S distances, thus minimizing repulsion. Thus, in a natural manner, surfaces in contact with a given H_2S/H_2 ratio form a refractory surface structure consisting of strongly-bound S-adlayers, but also adsorb molecules and more weakly-bound S in the interstitial spaces within the template. The Langmuirian kinetic treatment that follows hereinforth treats these interstices as the uncovered working surface and uses the number of interstices as the number of *accessible* sites, onto which all intermediates are able to bind in the reversible manner required for catalytic turnovers. Such constructs are also applicable to ReS_x surfaces, for which some S-atoms can be reversibly removed, until

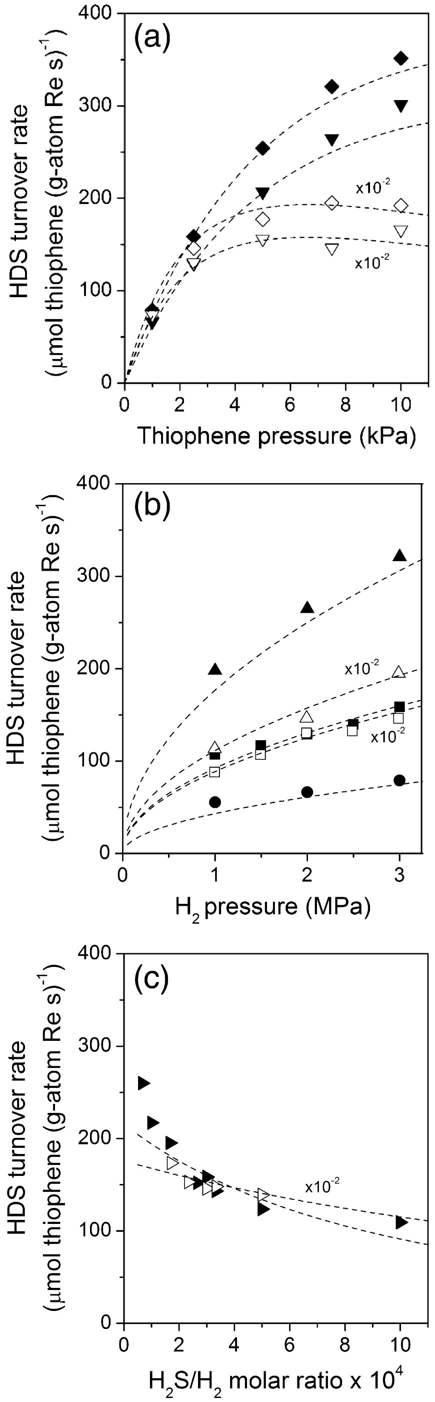

Fig. 9. Hydrodesulfurization turnover rates of thiophene consumption on 13.5% wt. Re/SiO_2 (closed symbols) and ReS_x/SiO_2 (open symbols, $\times 10^{-2}$) at 573 K as a function of (a) thiophene pressure at 2.0 MPa (▼) and 3.0 MPa (◆) H_2, 0.0003 H_2S/H_2 ratio, of (b) H_2 pressure at 1.0 kPa (●), 2.5 kPa (■), and 7.5 kPa (▲) thiophene, 0.0003 H_2S/H_2 ratio, and of (c) H_2S/H_2 ratio at 3.0 MPa H_2, 2.5 kPa thiophene (►). Curves reflect regression of all measured data to the functional form of Eq. (9).

the structures form the uncovered working surface in the kinetic treatments that follow. In all cases, such sites are assumed to bind the species described in Scheme 2 in a manner that does not depend on the coverage by other species, set by the thermodynamics of adsorption of H_2, H_2S, and thiophene in their various adsorbed forms.

THT and C_4 products both form as primary products on the active interstices within such refractory templates; the ratio of THT and C_4 products did not depend on thiophene pressure or H_2S/H_2 ratio (Figs. 8 and S.7-1), even when adsorbed species derived from thiophene and H_2S coexisted on the surface and H_2S/H_2 strongly inhibited rates (Fig. 9a and c). Thus, THT and C_4 formation rates sense the occupancy of the sites by different species to similar extents, indicative of the involvement of the same site and possibly of common intermediates, in these two reaction outcomes.

Total HDS rates increased with increasing H_2 and thiophene pressures (Fig. 9a and b) and decreased with increasing H_2S/H_2 ratios (Fig. 9c) in a manner consistent with the rate equation:

$$\frac{r}{[L]} = \frac{\alpha(H_2)^{0.5}(T)}{\left(\underset{(*)}{1} + \underset{(T^*)}{\beta(T)} + \underset{(H^*)}{\gamma(H_2)^{0.5}} + \underset{(H_2S^*)}{\delta(H_2S)} + \underset{(HS^*)}{\epsilon\frac{(H_2S)}{(H_2)^{0.5}}} + \underset{(S^*)}{\eta\frac{(H_2S)}{(H_2)}}\right)^2} \tag{5}$$

The denominator terms of Eq. (5) reflect the respective site occupancies by adsorbed species through a balance equation for active sites:

$$\begin{aligned}[L] &= (*) + (T*) + (H*) + (H_2S*) + (HS*) + (S*) \\ &= (*)\cdot\left(1 + \beta(T) + \gamma(H_2)^{0.5} + \delta\,(H_2S) + \epsilon\frac{(H_2S)}{(H_2)^{0.5}} + \eta\frac{(H_2S)}{(H_2)}\right)\end{aligned} \tag{6}$$

where [L] represents the total number of sites within the surface template and (*) denotes those interstices that remain unoccupied during steady-state catalysis. This equation is consistent with the elementary steps in Scheme 2, with quasi-equilibrium assumptions that render the addition of a hydrogen species (H^*) to an adsorbed thiophene intermediate (T^*) the sole kinetically-relevant step. This mechanistic interpretation brings chemical significance to the parameters in Eqs. (5) and (6):

$$\alpha = k_0 K_{H_2}^{0.5} K_T \tag{7a}$$

$$\beta = K_T \tag{7b}$$

$$\gamma = K_{H_2}^{0.5} \tag{7c}$$

$$\delta = K_{H_2S} \tag{7d}$$

$$\epsilon = \frac{K_{H_2S}K_{HS}}{K_{H_2}^{0.5}} \tag{7e}$$

$$\eta = \frac{K_S K_{H_2S} K_{HS}}{K_{H_2}} \tag{7f}$$

Eq. (5) accurately describes the combined rates of formation of THT and C_4, but not their individual rates, because their relative rates reflect a kinetic branching point that dictates the fate of a common intermediate after the kinetically-relevant step. A previous proposal [17,18] supposes the involvement of parallel routes to THT and C_4 via different reactive intermediates at rates that must depend similarly on H_2 and thiophene pressures, indicative of kinetically-relevant transition state structures of similar molecularity, but possibly with a different atomic connectivity that would dictate the products formed. Measured primary selectivities

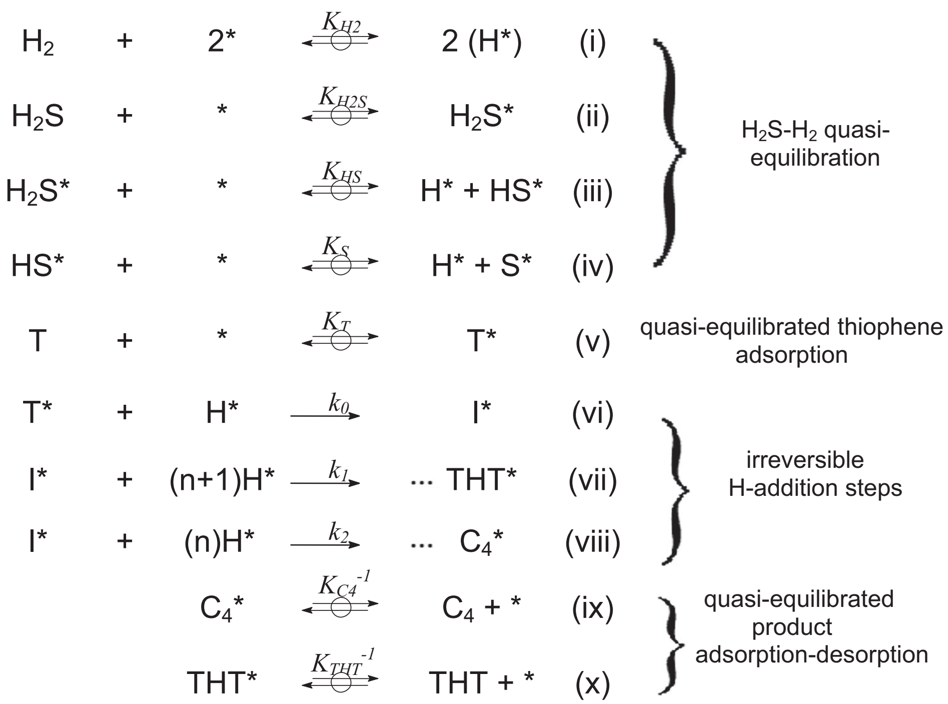

Scheme 2. Elementary steps for thiophene HDS and desulfurization-hydrogenation pathways. Surface species bound on *, which are interstitial binding sites retained on refractory surface templates of S-adatoms formed on Re and ReS_x, include hydrogen (H^*), hydrogen sulfide (H_2S^*), sulfhydryl (HS^*), sulfur (S^*), and thiophene (T^*). These species are derived from quasi-equilibrated H_2S-H_2 (*steps i-iv*) and thiophene (*step v*) adsorption steps. Thiophene conversion rates are mediated by the kinetic coupling of T^* and H^* (*step vi*), which forms a common reaction intermediate (I^*). Tetrahydrothiophene (THT) and butene/butane (C_4) products form from I^*, via subsequent surface reactions that may involve one or more (i.e., *n*, *n + 1*, etc.) H-atom addition steps (*steps vii* and *viii*), and desorb from * (*steps ix* and *x*). Selectivity data indicate the transition state structure that mediates THT formation involves one more H-atom (i.e., *n + 1*, *step vii*) than the transition state that mediates C_4 formation (*step viii*).

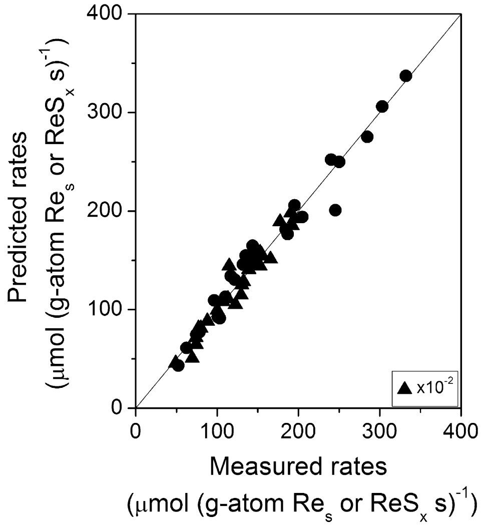

Fig. 10. Parity plot of measured hydrodesulfurization rates and those determined by regression of all data to the functional form of Eq. (9) on 13.5% wt. Re/SiO$_2$ (●) and ReS$_x$/SiO$_2$ ($\times 10^{-2}$) (▲) at 573 K, with the regressed parameters listed in Table 2.

to THT and C$_4$, however, depend on H$_2$ pressure (Fig. 8a and b; also Section 3.5); THT and C$_4$ must therefore form via two distinct transition states with a different number of H-atoms. The ability to describe their combined formation rates using Eq. (5) then would require a fortuitous coincidence that would have to persist over a significant range of thiophene, H$_2$ and H$_2$S pressures (Fig. 10). We consider instead a common kinetically-relevant step for thiophene activation, leading to an intermediate (I*) that undergoes subsequent H-addition or C—S cleavage steps to form THT and C$_4$ products (Section 3.5).

Some of the terms in the denominator of Eq. (5) represent minority intermediates or spectators present at much lower coverages than other species. We consider first the relative coverages of H$_2$S-derived intermediates (H$_2$S*, HS*, and H*), as they form via the equilibration of gaseous H$_2$S and H$_2$. At each thiophene pressure, HDS rates normalized by (H$_2$)$^{0.5}$(T) (as dictated by the form of Eq. (5)) are single-valued functions of H$_2$S/H$_2$ ratios (SI, S.8, Fig. S.8-1), indicating that S* species prevail over those retaining H-atoms (HS*, H$_2$S*) and that S-chemical potentials at surfaces are set by H$_2$S/H$_2$ ratios. THT and C$_4$ selectivities (Fig. 8) were affected by thiophene conversion and residence time, but not by H$_2$S/H$_2$ ratios, in spite of their strong inhibition of turnover rates as S* coverages increase (Fig. 9c), indicating that THT and C$_4$ pathways do not depend differently on H$_2$S or H$_2$S/H$_2$ and therefore on S* coverages. H$_2$S dissociation to form S* and H* occurs via equilibrated sequences:

$$H_2S(g) + * \rightleftharpoons H_2S* \tag{8a}$$

$$H_2S(g) + * \rightleftharpoons HS * + \frac{1}{2}H_2(g) \tag{8b}$$

$$H_2S(g) + * \rightleftharpoons S * + H_2(g) \tag{8c}$$

Thus, the prevalence of S* over HS* and H$_2$S* also appears to be driven by entropy, as its formation leads to the evolution of one H$_2$(g) molecule (Eq. (8c)).

The ability of Eq. (5), with S* as the most abundant H$_2$S-derived bound species (i.e., $\delta = \varepsilon = 0$) and with the remaining adsorbate species (H*, T*), to describe HDS rates was examined by non-linear regression and sensitivity analysis methods [17,18] (SI, S.9). The relative magnitudes of the H*, T*, and S* terms in the denominator of Eq. (5) were determined, and the regression errors were insensitive to the value of γ, indicating that H* coverages are much smaller than for T*, S*, or * on both Re and ReS$_x$:

$$\frac{r}{[L]} = \frac{\alpha (H_2)^{0.5}(T)}{\left(\underset{(*)}{1} + \underset{(T*)}{\beta(T)} + \underset{(S*)}{\eta \frac{(H_2S)}{(H_2)}}\right)^2} \tag{9}$$

This equation accurately describes all rate data over a 100-fold range in rates for Re and ReS$_x$ catalysts and a broad and relevant range of conditions (1–3 MPa H$_2$, 1–10 kPa thiophene, 7–100 $\times 10^{-5}$ H$_2$S/H$_2$; Fig. 10). The large differences in turnover rates (>100-fold) between Re and ReS$_x$ thus reflect different kinetic and thermodynamic parameters in Eq. (9), instead of elementary steps that differ in identity or kinetic relevance. The regressed values of α, β, and η are shown in Table 2 for Re/SiO$_2$ and ReS$_x$/SiO$_2$ (13.5% wt. Re); they are examined in the context of their sensitivity to binding properties, and specifically to M—S bond energies, in Section 3.6. Next, we address, however, matters of selectivity in the context of primary and secondary routes to THT and C$_4$ products in order to assess the nature and selectivity of the kinetic branching point that dictates the products that form from the common reactive intermediate I*.

3.5. Primary and secondary routes to tetrahydrothiophene and C$_4$ products on Re and ReS$_x$

Measured THT/C$_4$ ratios decreased as conversion increased with increasing residence time but did not depend on thiophene pressures or H$_2$S/H$_2$ ratios (Figs. 8 and S.7-1), consistent with their formation on the same active sites at coverages that lead to the same denominator terms in their rate equations (Section 3.4). THT and C$_4$ formation rates depend differently on H$_2$ pressure (Fig. 8a and b) but not as a result of differences in their respective denominator terms (Eq. (9)). Their different numerator terms must reflect a different number of H-atoms in the transition states that mediate the conversion of I* to THT and C$_4$.

These product formation rates are discussed using the network depicted in Scheme 1 for the kinetically-relevant formation of I* species, which limits total thiophene conversion rates, and for their subsequent reactions, which determine the selectivity to THT and C$_4$ products. These steps lead to first-order rates for the consumption of I* (Eqs. (10) and (11)) with rate constants that depend on H$_2$ pressure, but which do not vary with residence time because H$_2$ is present in large stoichiometric excess. The rates of these primary paths, r$_1$ and r$_2$ at each H$_2$ pressure, are given by:

$$r_1 = k_1 \cdot (H_2)^{\frac{w}{2}}(*)(I*) = k_1'(*)(I*) \tag{10}$$

$$r_2 = k_2 \cdot (H_2)^{\frac{y}{2}}(*)(I*) = k_2'(*)(I*) \tag{11}$$

where *w* and *y* must be integers, reflecting the number of H-atoms added to I* in forming the transition states leading to THT and C$_4$, respectively. Their different values, and thus the different effects of H$_2$ on k′$_1$ and k′$_2$, account for the effects of H$_2$ on primary THT and C$_4$ selectivities (Fig. 8a and b).

Table 2
Kinetic parameters for thiophene hydrodesulfurization rates on 13.5% wt. Re/SiO$_2$ and ReS$_x$/SiO$_2$ from regression of kinetic data to the functional form of Eq. (9) at 573 K.

Thermodynamic/Kinetic Parameter	Re	ReS$_x$
$\alpha = k_0 K_{H2}^{0.5} K_T$ (s^{-1} kPa$^{-1.5}$)	2.2 (±0.4) $\times 10^{-6}$	2.6 (±0.5) $\times 10^{-4}$
$\beta = K_T$ (kPa^{-1})	6.8 (±1.2) $\times 10^{-2}$	1.7 (±0.2) $\times 10^{-1}$
$\eta = K_S K_{H2S} K_{HS} / K_{H2}$ (unitless)	6.3 (±1.9) $\times 10^{2}$	3.3 (±2.6) $\times 10^{2}$

Uncertainty (±) in reported values reflects 95% confidence level.

The readsorption of THT onto the sites on which it formed provides another opportunity to form the transition state that mediates C_4 formation via secondary reactions, evident from the observed residence time effects on THT/C_4 ratios (Fig. 8; also Section 3.3). Such reactions occur at rates (r_3) given by:

$$r_3 = k_3 \cdot (H_2)^{\frac{z}{2}}(*)(THT*) = k_3'(*)(THT*) \tag{12}$$

where (THT^*) is the coverage of bound tetrahydrothiophene in equilibrium with THT(g) (Scheme 2, *step x*), and *z* is the number of H-atoms added to THT^* in forming the transition state for C—S cleavage.

Eqs. (10)–(12) lead to product formation rates given by:

$$\frac{d(THT*)}{d\tau} = k_1 \cdot (H_2)^{\frac{w}{2}}(*)(I*) - k_3 \cdot (H_2)^{\frac{z}{2}}(*)(THT*) \tag{13}$$

$$\frac{d(C_4*)}{d\tau} = k_2 \cdot (H_2)^{\frac{y}{2}}(*)(I*) + k_3 \cdot (H_2)^{\frac{z}{2}}(*)(THT*) \tag{14}$$

These equations can be solved by assuming pseudo-steady state concentrations for I^*, which forms at rates given by Eq. (9) and reacts at rates given by Eqs. (10) and (11):

$$\frac{d(I*)}{d\tau} = r - \left[k_1 \cdot (H_2)^{\frac{w}{2}}(*) + k_2 \cdot (H_2)^{\frac{y}{2}}(*)\right] \cdot (I*) = 0 \tag{15}$$

Eqs. (13)–(15) describe how THT and C_4 concentrations vary with thiophene conversion (X) (SI, S.10). THT selectivity (the ratio of THT formed per thiophene converted) is then given by:

$$S_{THT} = \frac{k_1(H_2)^{\frac{w}{2}}}{k_1(H_2)^{\frac{w}{2}} + k_2(H_2)^{\frac{y}{2}}} \cdot \left(\frac{k_3(H_2)^{\frac{z}{2}}}{k_0K_{H2}^{0.5}(H_2)^{0.5}K_T} - 1\right)^{-1} \cdot \frac{\left\{(1-X) - (1-X)^{\frac{k_3(H_2)^{\frac{z}{2}}}{k_0K_{H2}^{0.5}(H_2)^{0.5}K_T}}\right\}}{X} \tag{16a}$$

where k_0 was defined previously as the rate constant for the kinetically-relevant coupling of T^* and H^* that determines total thiophene conversion rates (Scheme 2, *step vi*).

The regression of THT selectivity data (Fig. 8) to the general functional form of Eq. (16a):

$$S_{THT} = \frac{a}{b-1} \cdot \frac{(1-X) - (1-X)^b}{X} \tag{16b}$$

leads to values for *a* and *b*, which are given by:

$$a = \frac{k_1'}{k_1' + k_2'} = \frac{k_1(H_2)^{\frac{w}{2}}}{k_1(H_2)^{\frac{w}{2}} + k_2(H_2)^{\frac{y}{2}}} \tag{16c}$$

$$b = \frac{k_3'}{k_0K_{H2}^{0.5}(H_2)^{0.5}K_T} = \frac{k_3(H_2)^{\frac{z}{2}}}{k_0K_{H2}^{0.5}(H_2)^{0.5}K_T} = \frac{k_3}{k_0K_{H2}^{0.5}K_T} \cdot (H_2)^{\delta} = \frac{r_3}{r}; \delta = \frac{1}{2}(z-1) \tag{16d}$$

Eq. (16d) represents the rate ratio of secondary THT desulfurization to primary thiophene consumption reactions. Rate ratios of primary THT to C_4 formation are described by rearranging Eq. (16c) into:

$$\frac{r_1}{r_2} = \frac{k_1'}{k_2'} = \frac{a}{1-a} = \frac{k_1(H_2)^{\frac{w}{2}}}{k_2(H_2)^{\frac{y}{2}}} = \frac{k_1}{k_2}(H_2)^{\lambda}; \lambda = \frac{1}{2}(w-y) \tag{17}$$

Regressed values of r_1/r_2 data gave a half-order dependence ($\lambda = 0.5$, Eq. (17)) on H_2 pressure (Fig. 11a; $k_1/k_2 = 0.023 \pm 0.002$ $kPa^{-0.5}$) for both Re and ReS_x, consistent with THT products that are favored over C_4 as H_2 pressure increases and with a THT transition state that contains one more H-atom than that for C—S cleavage to form C_4 (i.e., (w-y) = 1, Eq. (17)). In contrast, r_3/r ratios depend inversely on H_2 pressure (Fig. 11b; $\delta = -1$, $z = -1$, Eq. (16d)), and THT desulfurization rates consequently exhibit a negative half-order dependence on H_2 (i.e., $z/2 = -0.5$, Eq. (12)). This negative H_2 dependence implies that removal of H-atoms from THT is required to cleave its C—S bond and form C_4. The sequential H-abstraction steps from THT:

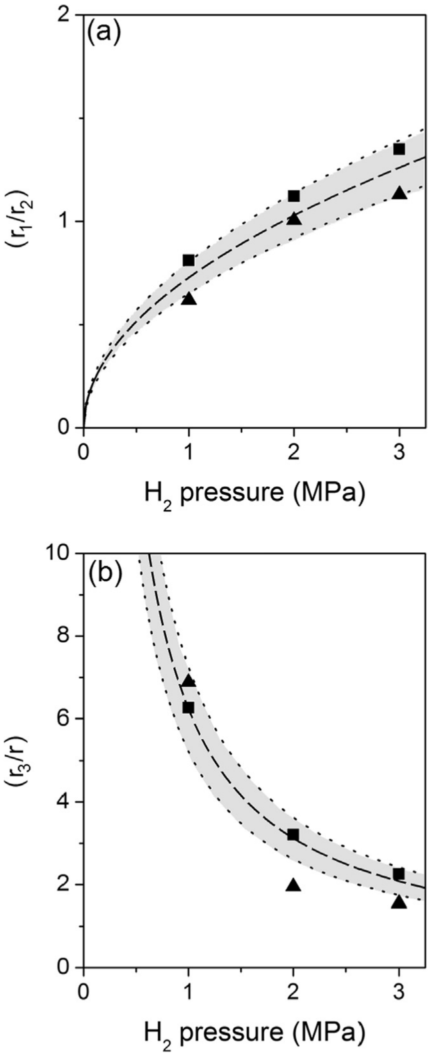

Fig. 11. Rate ratios of (a) primary THT to primary C_4 formation rates (r_1/r_2) and (b) secondary THT desulfurization to primary thiophene conversion rates (r_3/r), from regressed parameters obtained from fitting selectivity data to Eq. (16a) for (13.5% wt.) Re/SiO_2 (■) and ReS_x/SiO_2 (▲) at 573 K. Dashed curves indicate the best fit of (r_1/r_2) and (r_3/r) ratios to Eqs. (17) and (16d), respectively. Lightly shaded regions reflect the 95% confidence intervals from the regression of (r_1/r_2) and (r_3/r) ratios to $\sim(H_2)^{0.5}$ and $\sim(H_2)^{-1.0}$, respectively.

$$THT(g) + * \rightleftharpoons THT* \tag{18}$$

$$THT * + * \rightleftharpoons TrHT * + H* \tag{19}$$

$$TrHT * + * \rightleftharpoons DHT * + H* \tag{20}$$

$$DHT * + * \rightleftharpoons MHT * + H* \tag{21}$$

are depicted in Scheme 3 (with I_1^*, I_2^*, I_3^*, and I_4^* for monohydrothiophene (MHT^*), dihydrothiophene (DHT^*), trihydrothiophene ($TrHT^*$), and THT^*). Rates that depend on $(H_2)^{-0.5}$ are consistent with a kinetically-relevant H-atom abstraction from $TrHT^*$ (Eq. (20)) and with all preceding steps (Eqs. (18) and (19)) being equilibrated.

These conclusions about the number of H-atoms in the transition states that mediate C—S bond cleavage in thiophene and in

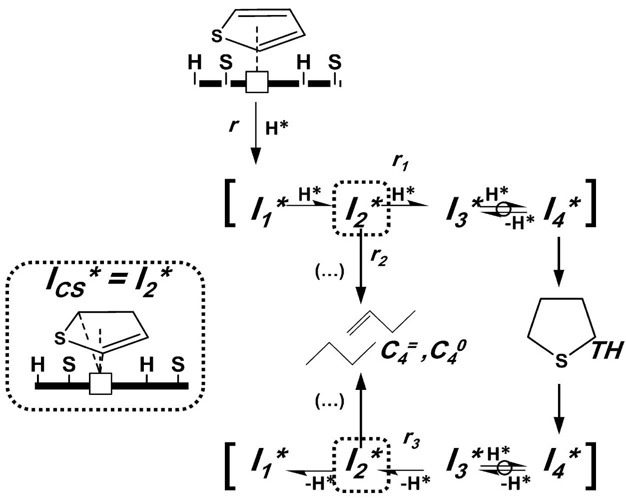

Scheme 3. Primary and secondary reactions on active interstices retained on refractory surface templates of S-adatoms formed on Re and ReS$_x$. Bound thiophene species undergo a kinetically-relevant H-atom (H*) addition, which mediates the rate of thiophene conversion, **r**. Partially-hydrogenated thiophene-derived surface intermediates are formed on the surface, denoted as I_n^*, where *n* indicates the number of added H-atoms relative to thiophene, and these intermediates form the transition states that mediate tetrahydrothiophene (THT; $\mathbf{r_1}$) and butene/butane ($C_4^=$, C_4^0; $\mathbf{r_2}$) formation. I_4^* desorbs as THT(g), and THT(g) readsorbs on (similar) surfaces to form $C_4^=$, C_4^0 ($\mathbf{r_3}$). Data indicates I_3^* species are quasi-equilibrated with THT (g), and rates of THT desulfurization ($\mathbf{r_3}$) are mediated by a kinetically-relevant H-atom abstraction from I_3^*. I_2^* is proposed to be the intermediate that undergoes C—S bond activation to form C$_4$ (i.e., I_{CS}^*); thus, a kinetically-relevant H-atom addition to I_2^* mediates primary THT formation ($\mathbf{r_1}$), consistent with r_1/r_2 ratios that exhibit a half-order H$_2$ dependence.

THT also inform the nature of the relevant intermediate (I_{CS}^*). The common intermediate in THT and C$_4$ formation (I^*) involves the kinetically-relevant addition of one H-atom to thiophene (Section 3.4); as a consequence, C$_4$ must form via a transition state that contains at least one more H-atom than thiophene (i.e., I_1^*, I_2^*, I_3^*, or I_4^* in Scheme 3). THT desulfurization rates exhibit a −0.5 order dependence on H$_2$ (Fig. 11b; $\delta = -1$, $z = -1$, Eq. (16d)), thus requiring the equilibration of I_3^* and I_4^* species with THT(g) (Eqs. (18) and (19) quasi-equilibrated). These I_3^* species either undergo a kinetically-relevant H-abstraction step (Eq. (20)), leading to the eventual formation of I_{CS}^*, which consequently contains fewer H-atoms than I_3^* (i.e., I_1^* or I_2^*), or act themselves as the I_{CS} species, subsequently forming the C—S bond scission transition state; both possibilities would lead to the observed H$_2$ dependence ($z/2 = -0.5$, Eq. (12)).

The ratio of primary THT to C$_4$ formation rates increases with H$_2$ pressure (Fig. 11a; $\lambda = 0.5$, Eq. (17)). These observations imply that a kinetically-relevant H-addition to I_{CS}^* must form the transition state that mediates THT formation, or, if I_3^* were to be the I_{CS} species, suggest that the equilibrated interconversion of I_3^* and THT(g) leads to THT/C$_4$ ratios that increase with H$_2$ pressure (Eqs. (18) and (19)). Such equilibration and the role of I_3^* as the precursor of C$_4$ products would lead to THT/C$_4$ ratios that depend on H$_2$ pressure but not on changes in conversion with residence time, in contradiction with experiments (Figs. 8 and S.7-1); as a result I_3^* cannot be the intermediate that leads to C—S cleavage (I_{CS}^*). I_{CS}^* represents instead a kinetic branching point for both C$_4$ and THT formation via respective transition states that differ in H-content. The C—S cleavage transition state may form from I_1^* or I_2^*; THT formation is mediated, in turn, by a kinetically-relevant H-addition step to this same I_{CS}^* moiety (I_1^* or I_2^*). If I_1^* is the I_{CS}^* moiety, H-addition would form I_2^* species (not in equilibrium with THT(g), based on the kinetics of THT desulfurization), which must undergo rapid hydrogenation steps to form THT. If I_2^* acts as I_{CS}^* and H-addition to I_2^* is kinetically-relevant, then the resulting I_3^* would form THT (g) via equilibrated steps (Eqs. (18) and (19)).

Irrespective of which hydrogenation step mediates the primary formation of THT, secondary C$_4$ formation from THT, which occurs upon re-forming I_{CS}^* on the surface, is mediated by the kinetically-relevant removal of H from I_3^* to form I_2^* (Fig. 11b; $\delta = -1$, $z = -1$, Eq. (16d)). The C—S bond cleavage transition state is then formed simply from the resulting intermediate (I_2^*) of this H-removal step (i.e., I_2^* is I_{CS}^*), or, if I_1^* is the I_{CS} moiety, is instead formed after an additional, rapid dehydrogenation step (of I_2^*). Thus, experimental evidence has narrowed the identity of I_{CS}^* to I_1^* or I_2^* but cannot alone discriminate between these two plausible outcomes. We adopt, here, the simpler mechanistic proposal of I_2^* as I_{CS}^*, which implies the presence of a kinetic barrier for the interconversion of I_2^* and I_3^*, which mediates THT primary formation and secondary desulfurization reactions.

THT formation, in the context of this mechanistic proposal, can be interpreted as an "overhydrogenation" mistake, caused by the addition of an additional H-atom to I_{CS}^*; such missteps can be corrected even after desorption as THT via its readsorption and dehydrogenation so as to re-form I_{CS}^*, which can then undergo C—S cleavage and S-removal. Irrespective of the specific identity of I_{CS}^*, C—S bond cleavage does require a species that contains more H-atoms than thiophene but fewer than THT. Such requirements for C—S bond cleavage are analogous to the H-removal steps required for C—C cleavage in (cyclo)alkane hydrogenolysis and C—O cleavage in alkanol deoxygenation [35–37], which are essential in weakening the bonds being cleaved and in providing an entropic driving force for the formation of the required transition states through the evolution of H$_2$(g). These reactions, irrespective of the identity of X in the C—X bonds, balance significant enthalpic barriers for C—X and C—H bond cleavage with gains in enthalpy and entropy via M—C bond formation and H$_2$ formation, respectively.

3.6. Consequences of M—S bond energies for HDS catalytic rates and selectivity and the role of active interstitial regions within refractory S* surface templates

Turnover rates differ markedly on Re and ReS$_x$ catalysts, in spite of their mediation of similar elementary steps (Sections 3.4 and 3.5), because their respective surfaces differ in the kinetic and thermodynamic parameters for such steps (in Eq. (9)). Different binding properties among catalysts are often invoked to explain HDS rate differences, a truism reinforced by the specific assignment of reactivity to M—S bond strengths, which must influence, but not always in a well-established manner, the rates of adsorption, bond activation, and desorption [13,21,22].

The equilibrium constant for S* formation (η in Eq. (7f)) reflects M—S bond energies, but η is only slightly smaller on ReS$_x$ (3.3 (±2.6) × 10^2) than on Re (6.3 (±1.9) × 10^2) (Table 2), a difference that is not likely to account for their 100-fold reactivity differences, which reflect instead their very different α values (2.2 (±0.4) × 10^{-6} s^{-1} kPa$^{-1.5}$ for Re and 2.6 (±0.5) × 10^{-4} s^{-1} kPa$^{-1.5}$ for ReS$_x$; Table 2). This α term represents a grouping ($k_0K_{H2}^{0.5}K_T$) of kinetic and thermodynamic terms (Scheme 2, *steps i*, *v*, and *vi*) and reflects the free energy difference ($\Delta G_{eff}^{\ddagger}$) between the transition state ($G^{\ddagger}$) for the kinetically-relevant step of thiophene consumption (Scheme 2, *step vi*) and the gaseous thiophene and H$_2$ reactants (G_T and G_{H_2}) and two vacant sites (G_*):

$$\alpha = k_0K_{H_2}^{0.5}K_T = \exp\left(-\frac{\Delta G_{eff}^{\ddagger}}{RT}\right) \tag{22}$$

$$\Delta G_{eff}^{\ddagger} = G^{\ddagger} - \left(2G_* + \frac{1}{2}G_{H_2} + G_T\right) \tag{23}$$

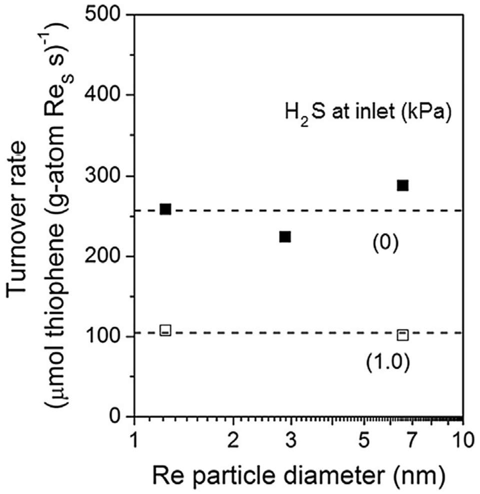

Fig. 12. Thiophene hydrodesulfurization turnover rates as a function of Re particle diameter (using Re dispersion, Table 1) of 0.97, 4.3, and 13.5% wt. Re/SiO$_2$ (3.0 MPa H$_2$, 2.5 kPa thiophene, 573 K) with 0 kPa (■) and 1.0 kPa (□) H$_2$S at the inlet.

The kinetically-relevant transition state contains a bound thiophene-derived species that is expected to be more stable and thus exhibit a lower free energy ($G^{\ddagger}$) as M—S bonds become stronger. Therefore, surfaces with stronger M—S bonds would, in fact, give smaller free energy differences between transition states and gaseous reactants ($\Delta G^{\ddagger}_{eff}$, Eq. (23)). Yet, α values are larger (and activation free energies smaller) on ReS$_x$ than Re, in spite of the stronger M—S bonds in the latter. These α values (Table 2), as normalized by the respective amounts of exposed surface areas, do not appear to reflect the intrinsic reactivity of such surfaces, possibly because the fraction of the surface that consists of the active interstices within refractory S^* templates differs between these two Re phases.

Available characterization and kinetic probes cannot definitively exclude the presence of very active ReS$_2$ surfaces or domains present at very low coverages on Re metal samples during exposure to H$_2$S/H$_2$ mixtures. Such domains are not detected by any of the methods used here, which showed that bulk ReS$_x$ does not form from Re^0 domains at the conditions of HDS catalysis (Section 3.1). Any spectroscopic or structural distinctions between ReS$_2$ domains and chemisorbed S-species on Re metal surfaces would therefore be speculative and cannot be falsified by experiment. We do expect, however, that such ReS$_2$ domains would respond in their concentration, S-stoichiometry, and structure to H$_2$S/H$_2$ ratio in a manner that is distinctly different from the response of lamellar ReS$_x$ structures dispersed on supports. As a result, kinetic responses to H$_2$S/H$_2$ ratios on Re metal and ReS$_x$ samples would differ, in contradiction with measurements (Table 2).

The assignment of kinetic and thermodynamic significance to $k_0K_{H2}^{0.5}K_T$ relies on an accurate normalization of measured HDS rates by the number of active sites. In contrast, equilibrium adsorption constants represent intrinsic values, independent of the number of such sites. The number of sites that can turnover, because they can reversibly bind reactants, products, and more specifically S^* atoms, remains inaccessible to experimental inquiry. The similar β and η thermodynamic parameters on Re and ReS$_x$ (Table 2) indicate that differences in the number of interstices in S^* templates, instead of binding energy differences, account for the different turnover rates on Re and ReS$_x$. Thus, M—S bond strengths at Re and ReS$_x$ surfaces dictate the fraction of their respective surfaces consisting of interstices capable of reversible S^* binding within templates formed by irreversibly-bound S^*.

These reversibly bound S^* species form as a natural consequence of their equilibrium with H$_2$S/H$_2$ at interstices within a template of strongly-bound S^* species. The fraction of the exposed surfaces that consist of such interstices is likely to be larger on surfaces that bind S more weakly, such as ReS$_x$. The size of catalytic particles can also influence their binding properties because smaller structures favor exposed atoms of lower-coordination, which bind adsorbates more strongly and form stronger M—S bonds. Such effects are most evident for particles in the 1–10 nm diameter range. It seems plausible that Re particles of this size would retain a different number of active interstices per surface area. Yet, thiophene HDS turnover rates were essentially the same for Re crystallites 1–7 nm in diameter (Fig. 12). These observations may indicate that the formation of refractory templates of strongly-bound S-adatoms dampens these structural non-uniformities expected from changes in the coordination of surface atoms and, in doing so, leads to surface structures with a similar fraction of active interstices. Such insensitivity to structures is reminiscent of those typical of surfaces nearly saturated with strongly-bound intermediates, as is the case for CO oxidation on Pt, for which the dense CO^* adlayers present lead to CO oxidation turnover rates and CO binding energies that do not depend on Pt crystallite size (1.2–20 nm) [77].

4. Conclusions

In contrast to Ru and Pt-based catalysts, Re and ReS$_x$ retained their initial phases upon exposure to a similar range of S-chemical potentials prevalent in HDS practice. Such phase integrity suggests the presence of formidable nucleation barriers that prevented their interconversions; these behaviors appear analogous to those observed in the formation of transition metal carbides and nitrides, which can readily form from their oxide precursors but can only form at very high supersaturations and temperatures from their respective metal clusters [78,79]. Such metastability exhibited by Re and ReS$_x$ thus permitted rigorous kinetic comparisons, at similar HDS conditions, without concurrent phase transformations.

Turnover rates on ReS$_x$, normalized by total Re atoms and thus reflecting a lower bound estimate, were 100-fold greater than those on Re, normalized by exposed Re atoms. Similar kinetic responses, selectivity trends, and measured adsorption constants were observed on both Re and ReS$_x$, indicating that differences in their measured rates are derived predominantly from differences in the number and not in the reactivity of accessible binding sites during steady-state catalysis. At relevant HDS conditions, refractory surface templates composed of strongly-bound S-adatoms form on catalyst surfaces; reactants and weakly-bound S-atoms then bind on the interstices retained within these templates. These active interstitial sites define the working surfaces on which reactive intermediates can bind reversibly, as required for catalytic turnovers. While the fraction of these active interstices within these refractory surface templates cannot be measured experimentally, the lower rates exhibited by Re suggest a greater dearth of binding sites, consistent with its stronger intrinsic M—S binding energy relative to ReS$_x$, and, in this way, the binding properties of the underlying bulk can influence measured HDS rates.

Tetrahydrothiophene (THT) and butene/butane (C$_4$) were formed on Re-based catalysts via pathways that occurred on similar types of sites. They form from partially-saturated thiophene surface intermediates, and their rates are mediated by transition state structures that differ by one H-atom. THT in the gas phase can also readsorb on the (same) surface and form C$_4$ products upon removal of some H-atoms, presumably to reform the surface intermediate that can undergo C—S bond activation. From such a perspective, THT formation represents an “overhydrogenation mistake,” for which the surface corrects via readsorption, H-abstraction, and subsequent C—S cleavage. Indeed, the prerequisites of H-removal steps observed here find precedence in C—C and C—O hydrogenolysis reactions of alkanes and alkanols, respectively [33–37], where they lead to enthalpic and entropic gains via C-metal bond formation and H_2 evolution, respectively, while weakening the C—C or C—O bond. These similar mechanistic features suggest that HDS represents a specific example of a broader class of C—X (X = C, O, S) bond scission reactions on crowded metal surfaces.

Acknowledgement

We acknowledge the financial support for this research from the Director, Office of Basic Energy Sciences, Chemical Sciences Division of the U.S. Department of Energy. We also acknowledge Dr. Huamin Wang for collecting XAS data on Re and ReS_x samples at the Stanford Synchrotron Radiation Lightsource and Dr. Sarika Goel for XRD measurements on Re and ReO_x samples at the College of Chemistry, University of California, Berkeley. We thank Dr. Sarika Goel for her careful review of this manuscript.

Appendix A. Supplementary material

Supplementary data associated with this article can be found, in the online version, at https://doi.org/10.1016/j.jcat.2018.03.031.

References

[1] H. Topsøe, B.S. Clausen, F.E. Massoth, Catalysis Science and Technology, Springer-Verlag, New York, 1996.
[2] M.J. Girgis, B.C. Gates, Ind. Eng. Chem. Res. 30 (1991) 2021.
[3] R. Prins, V.H.J. de Beer, G.A. Somorjai, Catal. Rev. 31 (1989) 1.
[4] S. Kasztelan, D. Guillaume, Ind. Eng. Chem. Res. 33 (1994) 203.
[5] A. Borgna, E.J.M. Hensen, J.A.R. van Veen, J.W. Niemantsverdriet, J. Catal. 221 (2004) 541, https://doi.org/10.1016/j.jcat.2003.09.018.
[6] F. Besenbacher, S. Helveg, J.V. Lauritsen, E. Laegsgaard, I. Stensgaard, J.K. Nørskov, B.S. Clausen, H. Topsøe, Phys. Rev. Lett. 84 (2000) 951.
[7] J.V. Lauritsen, J. Kibsgaard, G.H. Olesen, P.G. Moses, B. Hinnemann, S. Helveg, J. K. Nørskov, B.S. Clausen, H. Topsøe, E. Laegsgaard, et al., J. Catal. 249 (2007) 220, https://doi.org/10.1016/j.jcat.2007.04.013.
[8] M. Neurock, R.A. van Santen, J. Am. Chem. Soc. 116 (1994) 4427.
[9] S. Brunet, A. Daudin, G. Perot, P. Raybaud, C. Bouchy, J. Catal. 248 (2007) 111, https://doi.org/10.1016/j.jcat.2007.03.009.
[10] F. Cesano, S. Bertarione, A. Piovano, G. Agostini, M.M. Rahman, E. Groppo, F. Bonino, D. Scarano, C. Lamberti, S. Bordiga, et al., Catal Sci. Technol. 1 (2011) 123, https://doi.org/10.1039/c0cy00050g.
[11] C.S. Song, Catal. Today 86 (2003) 211, https://doi.org/10.1016/S0920-5861(03), 00412-7.
[12] A. Stanislaus, A. Marafi, M.S. Rana, Catal. Today 153 (2010) 1, https://doi.org/10.1016/j.cattod.2010.05.011.
[13] T.A. Pecoraro, R.R. Chianelli, J. Catal. 67 (1981) 430.
[14] M. Lacroix, N. Boutarfa, C. Guillard, M. Vrinat, M. Breysse, J. Catal. 120 (1989) 473.
[15] A. Niquille-Röthlisberger, R. Prins, J. Catal. 242 (2006) 207, https://doi.org/10.1016/j.jcat.2006.06.009.
[16] E.J.M. Hensen, H.J.A. Brans, G.M.H.J. Lardinois, V.H.J. de Beer, J.A.R. van Veen, R. A. van Santen, J. Catal. 192 (2000) 98, https://doi.org/10.1006/jcat.2000.2824.
[17] H. Wang, E. Iglesia, J. Catal. 273 (2010) 245, https://doi.org/10.1016/j.jcat.2010.05.019.
[18] H.-M. Wang, E. Iglesia, ChemCatChem 3 (2011) 1166, https://doi.org/10.1002/cctc.201100027.
[19] J. Quartararo, S. Mignard, S. Kasztelan, J. Catal. 192 (2000) 307, https://doi.org/10.1006/jcat.2000.2825.
[20] A. Ishihara, F. Dumeignil, J. Lee, K. Mitsuhashi, E.W. Qian, T. Kabe, Appl. Catal., A. 289 (2005) 163, https://doi.org/10.1016/j.apcata.2005.04.056.
[21] J.K. Nørskov, B.S. Clausen, H. Topsøe, Catal. Lett. 13 (1992) 1.
[22] H. Toulhoat, P. Raybaud, J. Catal. 216 (2003) 63, https://doi.org/10.1016/s0021-9517(02), 00118-5.
[23] C.J.H. Jacobsen, E. Törnqvist, H. Topsøe, Catal. Lett. 63 (1999) 179.
[24] H.C. Yao, M. Shelef, J. Catal. 44 (1976) 392, https://doi.org/10.1016/0021-9517(76), 90416-4.
[25] G.W. Chadzyñski, H. Kubicka, Thermochimica Acta 158 (1990) 369, https://doi.org/10.1016/0040-6031(90)80084-C.
[26] J. Okal, W. Tylus, L. Kepinski, J. Catal. 225 (2004) 498, https://doi.org/10.1016/j.jcat.2004.05.004.
[27] E.J.M. Hensen, P.J. Kooyman, Y. van der Meer, A.M. van der Kraan, V.H.J. de Beer, J.A.R. van Veen, R.A. van Santen, J. Catal. 199 (2001) 224, https://doi.org/10.1006/jcat.2000.3158.
[28] S. Shatynski, Oxid. Met. 11 (1977) 307, https://doi.org/10.1007/bf00608014.
[29] T.C. Ho, Q. Shen, J.M. McConnachie, C.E. Kliewer, J. Catal. 276 (2010) 114, https://doi.org/10.1016/j.jcat.2010.09.005.
[30] C.H. Bartholomew, P.K. Agrawal, J.R. Katzer, Adv. Catal. 31 (1982) 135.
[31] N.Y. Topsøe, H. Topsøe, J. Catal. 139 (1993) 641, https://doi.org/10.1006/jcat.1993.1056.
[32] T.I. Korányi, F. Moreau, V.V. Rozanov, E.A. Rozanova, J. Mol. Struct. 410–411 (1997) 103, https://doi.org/10.1016/S0022-2860(96), 09484-7.
[33] D.W. Flaherty, E. Iglesia, J. Am. Chem. Soc. 135 (2013) 18586, https://doi.org/10.1021/ja4093743.
[34] D.W. Flaherty, D.D. Hibbitts, E.I. Gürbüz, E. Iglesia, J. Catal. 311 (2014) 350, https://doi.org/10.1016/j.jcat.2013.11.026.
[35] D.W. Flaherty, D.D. Hibbitts, E. Iglesia, J. Am. Chem. Soc. 136 (2014) 9664, https://doi.org/10.1021/ja5037429.
[36] D.W. Flaherty, A. Uzun, E. Iglesia, J. Phys. Chem. C 119 (2015) 2597, https://doi.org/10.1021/jp511688x.
[37] E.I. Gürbüz, D.D. Hibbitts, E. Iglesia, J. Am. Chem. Soc. 137 (2015) 11984, https://doi.org/10.1021/jacs.5b05361.
[38] P. Arnoldy, J.A.M. van den Heijkant, V.H.J. de Beer, J.A. Moulijn, Appl. Catal. 23 (1986) 81, https://doi.org/10.1016/s0166-9834(00), 81454-2.
[39] D.J.C. Yates, J.H. Sinfelt, J. Catal. 14 (1969) 182, https://doi.org/10.1016/0021-9517(69), 90423-0.
[40] P. Arnoldy, E.M. van Oers, V.H.J. de Beer, J.A. Moulijn, R. Prins, Appl. Catal. 48 (1989) 241, https://doi.org/10.1016/s0166-9834(00), 82796-7.
[41] P. Arnoldy, E.M. van Oers, O.S.L. Bruinsma, V.H.J. de Beer, J.A. Moulijn, J. Catal. 93 (1985) 231, https://doi.org/10.1016/0021-9517(85)90171-x.
[42] C. Sepulveda, V. Belliere, D. Laurenti, N. Escalona, R. Garcia, C. Geantet, M. Vrinat, Appl. Catal., A 393 (2011) 288, https://doi.org/10.1016/j.apcata.2010.12.008.
[43] , Wiley-VHC, Weinheim, Germany, 2008.
[44] L. Lutterotti, M. Bortolotti, G. Ischia, I. Lonardelli, H.R. Wenk, Zeitschrift für Kristallographie Suppl. 2007 (2007) 125, https://doi.org/10.1524/zksu.2007.2007.suppl_26.125.
[45] B. Ravel, Athena: XAS, Data Process. (9) (2016) 26.
[46] B. Ravel, Artemis: EXAFS Data Analysis using Feff with Larch or Ifeffit, 2016, 0.9.26.
[47] H.H. Murray, S.P. Kelty, R.R. Chianelli, C.S. Day, Inorg. Chem. 33 (1994) 4418, https://doi.org/10.1021/ic00097a037.
[48] N. Yang, G.E. Mickelson, N. Greenlay, S.D. Kelly, F.D. Vila, J. Kas, J.J. Rehr, S.R. Bare, AIP Conf. Proc. 882 (2007) 591.
[49] D.C. Koningsberger, R. Prins, X-ray Absorption: Principles, Applications, Techniques of EXAFS, SEXAFS, and XANES, Wiley, New York, 1988.
[50] J.A. van Bokhoven, C. Lamberti, X-Ray Absorption and X-Ray Emission Spectroscopy: Theory and Applications, Wiley, 2016.
[51] J.J. Rehr, J.J. Kas, F.D. Vila, M.P. Prange, K. Jorissen, PCCP 12 (2010) 5503, https://doi.org/10.1039/b926434e.
[52] D.E. Mears, Ind. Eng. Chem. Process Des. Dev. 10 (1971) 541, https://doi.org/10.1021/i260040a020.
[53] M. Bai, Z.-H. Liu, L.-J. Zhou, Z.-Y. Liu, C.-F. Zhang, Trans. Nonferrous Met. Soc. China. 23 (2013) 538, https://doi.org/10.1016/s1003-6326(13), 62496-6.
[54] W.T. Tysoe, F. Zaera, G.A. Somorjai, Surf. Sci. 200 (1988) 1, https://doi.org/10.1016/0039-6028(88), 90428-1.
[55] B. Mitra, X. Gao, I.E. Wachs, A.M. Hirt, G. Deo, PCCP 3 (2001) 1144, https://doi.org/10.1039/b007381o.
[56] J. Benard, J. Oudar, N. Barbouth, E. Margot, Y. Berthier, Surf. Sci. 88 (1979) L35, https://doi.org/10.1016/0039-6028(79), 90094-3.
[57] H. Windawi, J.R. Katzer, Surf. Sci. 75 (1978) L761, https://doi.org/10.1016/0039-6028(78), 90192-9.
[58] H. Windawi, J.R. Katzer, J. Vacuum Sci. Technol. 16 (1979) 497, https://doi.org/10.1116/1.570019.
[59] E.B. Maxted, Adv. Catal. 2 (1951) 129.
[60] H. Kubicka, J. Catal. 12 (1968) 223, https://doi.org/10.1016/0021-9517(68), 90102-4.
[61] B.H. Isaacs, E.E. Petersen, J. Catal. 85 (1984) 1, https://doi.org/10.1016/0021-9517(84), 90103-9.
[62] G.W. Chądzyñski, H. Kubicka, Thermochim. Acta. 158 (1990) 353.
[63] W. Zmierczak, G. MuraliDhar, F.E. Massoth, J. Catal. 77 (1982) 432, https://doi.org/10.1016/0021-9517(82), 90184-1.
[64] M. Daage, R.R. Chianelli, J. Catal. 149 (1994) 414, https://doi.org/10.1006/jcat.1994.1308.
[65] A. Niquille-Roethlisberger, R. Prins, Catal. Today 123 (2007) 198, https://doi.org/10.1016/j.cattod.2007.01.053.
[66] G. Berhault, M. Lacroix, M. Breysse, F. Mauge, J.-C. Lavalley, L. Qu, J. Catal. 170 (1997) 37, https://doi.org/10.1006/jcat.1997.1733.
[67] G. Berhault, M. Lacroix, M. Breysse, F. Mauge, J.-C. Lavalley, H. Nie, L. Qu, J. Catal. 178 (1998) 555, https://doi.org/10.1006/jcat.1998.2196.
[68] R.J. Madon, H. Shaw, Catal. Rev. – Sci. Eng. 15 (1977) 69, https://doi.org/10.1080/03602457708081722.
[69] J. Oudar, Catal. Rev. – Sci. Eng. 22 (1980) 171.
[70] H.A. Yoon, N. Materer, M. Salmeron, M.A. Van Hove, G.A. Somorjai, Surf. Sci. 376 (1997) 254, https://doi.org/10.1016/S0039-6028(96), 01405-7.

[71] D.G. Kelly, A.J. Gellman, M. Salmeron, G.A. Somorjai, V. Maurice, M. Huber, J. Oudar, Surf. Sci. 204 (1988) 1, https://doi.org/10.1016/0039-6028(88), 90264-6.

[72] J.G. McCarty, H. Wise, J. Chem. Phys. 72 (1980) 6332, https://doi.org/10.1063/1.439156.

[73] J.G. McCarty, H. Wise, J. Chem. Phys. 74 (1981) 5877, https://doi.org/10.1063/1.440905.

[74] J.G. McCarty, H. Wise, J. Chem. Phys. 76 (1982) 1162, https://doi.org/10.1063/1.443085.

[75] J.G. McCarty, K.M. Sancier, H. Wise, J. Catal. 82 (1983) 92, https://doi.org/10.1016/0021-9517(83), 90120-3.

[76] J.G. McCarty, H. Wise, J. Catal. 94 (1985) 543, https://doi.org/10.1016/0021-9517(85), 90218-0.

[77] A.D. Allian, K. Takanabe, K.L. Fujdala, X. Hao, T.J. Truex, J. Cai, C. Buda, M. Neurock, E. Iglesia, J. Am. Chem. Soc. 133 (2011) 4498, https://doi.org/10.1021/ja110073u.

[78] S.T. Oyama, Catal. Today 15 (1992) 179, https://doi.org/10.1016/0920-5861(92)80175-M.

[79] L. Volpe, M. Boudart, J. Solid State Chem. 59 (1985) 332, https://doi.org/10.1016/0022-4596(85), 90301-9.